Master's Theses and Capstones   Student Scholarship

Fall 2011

A two-dimensional hexagonal network model of alveolar mechanics

Danielle Nangle
University of New Hampshire, Durham

A TWO-DIMENSIONAL HEXAGONAL NETWORK MODEL OF ALVEOLAR
MECHANICS

BY

DANIELLE NANGLE
B.S. Biomedical Engineering Georgia Institute of Technology, 2008

THESIS

Submitted to the University of New Hampshire in the Partial Fulfillment of the
Requirements for the Degree of

Master of Science

In

Mechanical Engineering

September 2011

UMI Number: 1504957

UMI®

Dissertation Publishing

ProQuest®

This thesis has been examined and approved.

Thesis Director, Gregory P. Chini
Associate Professor Mechanical Engineering

Nivedita Gupta
Associate Professor Chemical Engineering

Chris White
Assistant Professor Mechanical Engineering

Date

Dedication

To my husband.

Acknowledgements

I would like to express my sincere gratitude to Dr. Greg Chini and Dr. Niva Gupta without whose guidance this thesis would not have been possible.

Contents

List of Tables

List of Figures

ABSTRACT

Alveolar Micromechanics
By

Danielle Nangle
University of New Hampshire, September, 2011

Pulmonary micromechanics (at the scale of alveoli) involves a delicate balance among tissue material properties, geometry, surface tension, pressure and stress distribution. To date, there is not a consensus among alveolar mechanics researchers about how these factors interact, in part because alveoli are so difficult to image and study *in vivo.* Here, we propose a basic mathematical model of a two-dimensional hexagonal network of mechanically coupled alveoli. We investigate equilibrium configurations of both dry and wet, internally pressurized elastic networks. Specifically, we compute pressure-area curves to quantify the differences among networks with different spring constants, internal pressures, network size and surface tensions. We conclude that a two-dimensional hexagonal network in force equilibrium is an appropriate first step in modeling the mechanics of the dynamic lung.

CHAPTER 1.

Introduction: Literature Review and Motivation

Section 1.1. What is the lung?

The mammalian lung is an organ which serves as the primary site of gas exchange that oxygenates the blood and removes carbon dioxide from the cardiovascular system. It also traps pathogens as part of mechanical immune defense (Guyton & Hall 1996). These core functions are fundamentally mechanical. The muscles attached to the rib cage and diaphragm expand and contract the lung, transmitting force throughout the parenchyma (lung body) to the alveoli (the smallest unit of the lung) (Ricci et al. 2002). When the lung is inflated, stresses are induced in the alveolar walls, or "septa" (Fung 1975b). Because gas is exchanged by diffusion, the alveolar walls must be thin; but they also must be strong enough to withstand *billions* of strain cycles (breaths) in a life time. Alveolar mechanics involves a delicate balance between structural stability and gas permeability: "That is to say that in the biological design of the pathway for oxygen there is little wasted structure and no over design" (Fredberg & Kamm 2006).

Remarkably, there are no attachments between the lung and the wall of the rib cage except where the pulmonary artery enters the lung. As a result, the lung

literally floats in the thoracic cavity surrounded by a thin layer of pleural fluid that lubricates movements of the lung within the cavity. A slight suction is maintained between the surface of the lung pleura and the surface of the thoracic cavity. Therefore the lungs are held to the thoracic wall as if glued there, except they can move freely as the chest expands and contracts (think of two damp microscope slides that are difficult to pull apart) (Guyton & Hall 1996).

Physiologically, the lung originates at the trachea in the throat. The trachea then bisects forming bronchioles which then arborize into terminal bronchioles which end in alveolar clusters. It is important to recognize that these clusters can be joined to one another so that in general there is no pressure difference in neighboring groups of alveoli.

The human lung is composed of about 500 million alveoli, which totals 90 square meters of surface area available for gas exchange (Fredberg & Kamm 2006, Weibel 2008)[1]. In the body, alveoli are irregular polygons with mutually shared walls between neighbors. They have been modeled with spheres, cubes, and shapes like dodecahedrons and 14-hedrons (see Figure 1). The mechanical properties of the alveolar walls will be discussed in a few paragraphs (Karakaplan et al. 1980).

---

[1]Another fascinating fact is that alveolar duct size and alveolar diameters are roughly the same across many animal species. Alveolar size is similar in the shrew and elephant even though body mass magnitude is a five-fold difference between the two (Fredberg & Kamm 2006).
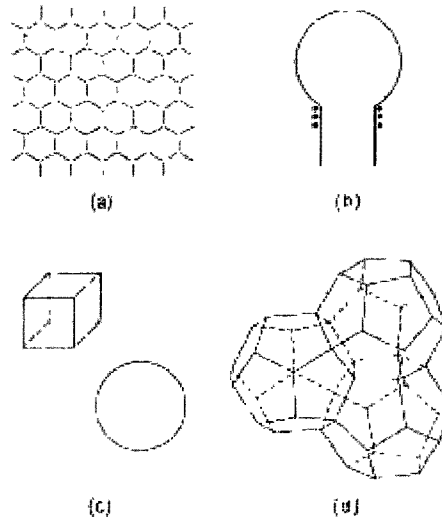
Figure 1: Shapes used to model alveoli (from Karakaplan et al. 1980).

Before we move to an introduction of lung mechanics, we would like to define

frequently used terms below in Table 1:

Term	Definition
Alveoli	The smallest unit of the lung and site of gas exchange
Septa	Alveolar wall; usually shared by two to four neighbors
Parenchyma	The main body of the lung
Pores of Kohn	Small pores in the septa that equalize pressure in neighboring alveoli
Alveolar Ducts	Smallest airways; they connect alveoli to primary airways (terminal bronchioles)
Liquid Lining	Thin liquid layer of fluid that coats the inside of an alveoli; there is not a consensus of the physiologic volume
Surfactant	Surface active agent that reduces surface tension of thin film lining (released by Type II alveolar cells)

Table 1: Frequently used terms.

As mentioned above, each alveolus shares its walls with its neighbors; this

aspect of alveolar structure has been termed "interdependence." Because of this,

an inhale or exhale causes stresses to be transmitted throughout the entire lung

from organ to cell to molecule (Fredberg & Kamm 2006). Parenchymal integrity is

3

ensured by the tension of the alveolar wall network (which itself is an interconnected network of collagen, elastin, fibrin, glycosaminoglycans, smooth muscle, and capillaries) (Weibel 2008, Suki et al. 2005).

Section 1.2. Introduction to alveolar mechanics

One way stress in the lung can be quantified is by measuring strain, defined as a resulting length change per initial length. During a human lifetime the lung as well as the cells within it must withstand 10^9 strain cycles with amplitudes that approach 4% during quiet tidal breathing and 10^7 strain cycles with amplitudes that approach 25% during sighs, deep inspirations, or heavy exercise (Fredberg & Kamm 2006). By classical engineering standards these loads would require robust structures, but since the primary purpose of the lung is gas exchange, thin membranes that allow diffusion are favored.

Stress can also be quantified by energy considerations. The parenchyma is viscoelastic due to the viscoelasticity of its constituents and thin film lining. Energetically, viscoelasticity means that any initial energy imposed on the system will be dissipated over time as the material "rearranges" itself toward a state of lower global energy (Bates 2007). In the case of the lung, an alveolar wall is exceptionally structurally complex (see Table 2). Because the lung parenchyma is viscoelastic, there are viscous losses during cycling (breathing). In reference to the septal wall alone (not including surface tension) it is thought that 10-20% of the energy of breathing is lost to friction between septal constituents. However it

is unknown how much energy is lost to the dynamic cycling of the thin film of fluid lining the lung (Fredberg & Kamm 2006).

Constituent	Function
Type I and II Collagen	Primary structural framework
Elastic fibers (elastin)	Secondary connective tissue
Microfibrils	Continuous, intertwined mantle around elastin fibers
ECM (extracellular matrix) and glycosaminoglycans	Provides structural support as a hydrated gel/ matrix in which connective tissues are embedded
Smooth muscle cells	Line and regulate patency of alveolar ducts and septal capillaries
Myofibroblasts and fibroblasts	Additional connective tissue also responsible for making ECM and some types of collagen

Table 2: Constituents of alveolar septa (from Suki et al. 2005).

Now that we have a basic understanding of lung physiology and mechanics we can discuss the following questions: What can go wrong with the lung? Why is it difficult to study the lung? And what are the disagreements about how the lung works?

Section 1.3. What can go wrong with the lung?

Because stress is concentrated as incident area decreases, an obstructed or collapsed alveoli or lung segment will put more stress on its neighbors. This increased stress greatly changes the local stress distribution, which means that parts of the lung that are not meant to bear loads may bear significant loads, potentially prompting a harmful feedback, in which inflammatory agents are released causing edema and possibly further degrading of lung tissue.

It is crucial to realize that healthy, normal alveoli *do not collapse* during normal

breathing (Fredberg & Kamm 2006, DiRocco et al. 2006, Wilson et al. 2001,

Fung 1975a, Hubmayr 2002). Alveolar collapse (also called atelectasis) is often

an indicator of disease or injury and is usually diagnosed when alveolar walls

collapse inward on themselves, so that internal sides of the alveoli come in

contact. Atelectasis is serious because it indicates that the interconnectedness of

the alveoli has been ruptured and that greater pressure is required to overcome

the surface tension of the fluid lining the septa that have collapsed onto each

other and "stick" together. Furthermore, injured lungs tend to have a larger shear

modulus which is thought to be due to edema, increased surface tension,

extracellular matrix remodeling, or scar formation (Faffe & Zin 2009). Table 3 lists

some primary lung diseases and malfunctions; the following text describes each

disease in detail.

Disease/ Problem	Impact	Statistics
ARDS-Adult Respiratory Distress Syndrome	Oxygen not transported to blood; can be caused by injury or disease	150,000 Americans will be diagnosed with acute respiratory distress syndrome each year and 42% of those will die from ARDS. (The ARDS Foundation 2011)
IRDS-Infant Respiratory Distress Syndrome	Infant mortality due to structural immaturity and lack of surfactant production	20 infant deaths in 100,000 in 2000 (The ARDS Foundation 2011)
Asthma	Inflammation and constriction of airways causing lack of oxygen transport	In the US, 7.7% of adults and 9.6% of children have asthma. There were 3,447 deaths due to asthma in 2007 (Centers for Disease Control and Prevention 2010).
Emphysema	A COPD- Chronic Obstructive Pulmonary Disease that destroys lung tissue causing less oxygen to be delivered to body	In the US, 4.9 million people were diagnosed and 12,790 people died in 2007 from emphysema (Centers for Disease Control and Prevention 2011). This disease increases lung compliance which causes the lung to become "floppy."
Pulmonary Fibrosis	The parenchyma becomes fibrous or scarred causing less oxygen to be delivered to body	200,000 adults have been diagnosed in the US in 2011 (Pulmonary Fibrosis Foundation 2011). This disease decreases lung compliance which causes the lung to become "stiff."
VILI- Ventilator Induced Lung Injury	Mechanical injuries due to overstretching of parenchyma; collapse and reopening of alveoli	Anyone with ARDS or ALI- Acute Lung Injury is susceptible to VILI
Pulmonary Edema	Fluid accumulation in lungs. If not treated sufferer will die of drowning	Occurs in 1-2% of the US population (MD Guidelines 2000)

Table 3: Table of most prevalent lung problems. See text for more details.

1.3.1 ARDS- Adult Respiratory Distress Syndrome

ARDS is a general term referring to any problem that causes breathing trouble and is usually caused by some kind of inflammation of the lung tissue; one example is that alveoli can collapse due to increased fluid or edema.

1.3.2 IRDS-Infant Respiratory Distress Syndrome

Although the name is similar to ARDS, IRDS has a specific cause. This type of respiratory distress is generally diagnosed in premature infants. It results when not enough surfactant is produced or is not of adequate concentration to coat the infant lung, decreasing the surface tension of the liquid lining to cause it to become patent after birth.

1.3.3 Asthma

Asthma is characterized by airway hyper-responsiveness and inflammation. This chronic inflammation is thought to cause tissue injury and structural remodeling in cells and tissue, manifesting as thickening airway walls, and increased collagen deposition making airways and septa less compliant. In contrast, elastase can be triggered to digest elastic fibers which would make airways more compliant (Faffe & Zin 2009). Because sub-bronchioles and alveolar ducts could be affected by asthma, a complete model of alveolar mechanics would incorporate the effects of hyper-responsiveness and inflammation on airways and alveoli.

1.3.4 Emphysema

Emphysema has been defined as an irreversible destruction of the alveoli and

airways causing increased lung compliance (see SEM of emphysematous lung in

Figure 2). Major mechanisms thought to be responsible for emphysema include

inflammatory agents, cell death in the alveolar walls, and extracellular matrix

remodeling among others (Faffe & Zin 2009). In animal models of emphysema,

elastase and collagenase is administered digesting the elastic fibers in the septal

walls (Brewer et al. 2003). The result is that after this treatment, the number of

intact collagen and elastin fibers decreases leading to a higher lung compliance

(Yuan et al. 2000). The danger is that highly compliant lung tissue collapses onto

itself, decreasing surface area for gas exchange and requiring greater pressure

to open the collapsed alveoli. In mammals, this to leads shorter, shallower

breaths and decreased oxygen delivery.

Normal   Emphysema
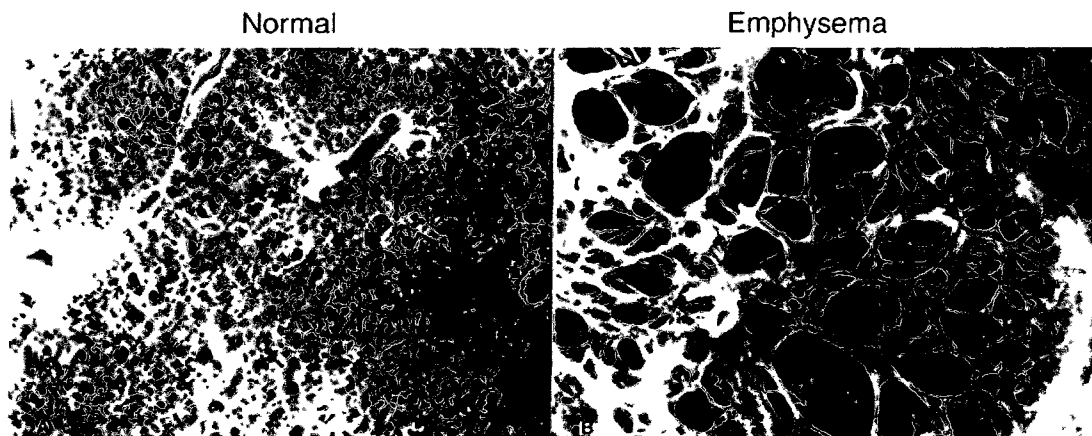
Figure 2: SEM of healthy (left) and emphysematous (right) lung (from Suki & Bates 2008).

Extensive study has been focused on what role the extracellular matrix plays in

emphysema. Suki & Bates (2008), used a 2D hexagonal spring network to model

9

a group of interconnected alveoli that was strained uniaxially (top and bottom).

To model emphysema some springs were either "cut" or certain spring constants

were randomly decreased relative to the spring constants of the remaining

springs. The yellow color in Figure 3 indicates springs experiencing high stress

and the blue, low stress.
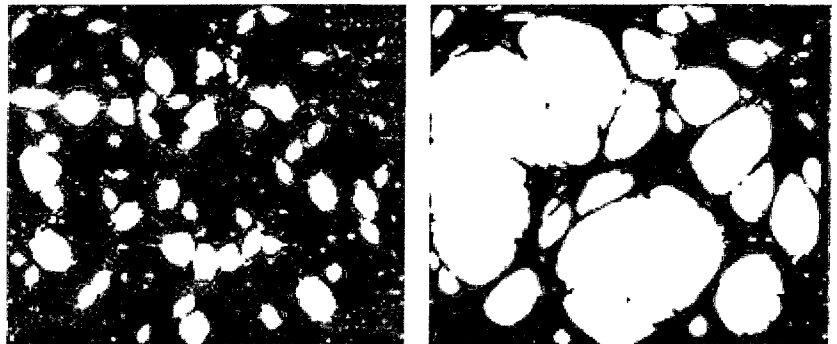
Figure 3: Hexagonal spring model, showing progression of emphysema (from (Suki & Bates 2008)

According to their model, the low stress picture to the far right shows that

extreme emphysema is characterized by very low stress in septal walls. In other

words, the emphysematous lung has very low compliance and can almost be

thought of as "floppy". Ito et al. (2005) conclude that collagen is significantly

remodeled in the alveolar wall, which produces many weak nonlinearly elastic

fibers. This causes the alveolar walls to fail and rupture leading to the holes like

those in the model of Suki & Bates (2008).

1.3.5 Pulmonary Fibrosis

Unlike emphysema, pulmonary fibrosis is characterized by excessive *production*

of collagen, elastin, and proteoglycans, which are constituents of alveolar walls

(Faffe & Zin 2009). This excess causes the septal walls to stiffen making

inhalation very difficult. If emphysema is characterized as slackening of the alveolar walls, pulmonary fibrosis is stiffening. Just as Suki and Bates (2008) investigated emphysema in a spring network model, they also analyzed pulmonary fibrosis using the same model, as seen in Figure 4.
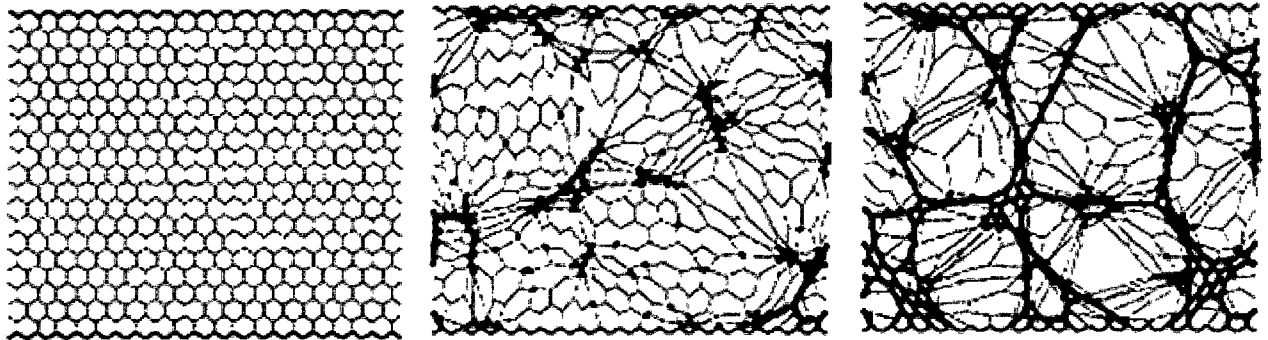
Figure 4: These three images show a progression of spring stiffness from uniform spring constants on the left to highly varied spring constants on the right (from Suki & Bates 2008).

In order to model pulmonary fibrosis, spring constants in the model were changed randomly to be stiffer than their neighbors. Eventually a few very stiff springs dominated the mechanics of the network, as seen in the far right picture of Figure 4. It has been hypothesized that increasing lung stiffness can also be triggered by areas of low oxygen or hypoxia, creating a feedback loop in the fibrosed lung (Sakai et al. 1999). In addition, the effects of age also stiffen lung tissue (Tanaka & Ludwig 1999, Lai-Fook & Hyatt 2000, Salerno & Ludwig 1999). To date, there is no way to reverse emphysema or pulmonary fibrosis (Suki & Bates 2008).

1.3.6 VILI-Ventilator Induced Lung Injury & pulmonary edema

A mechanically induced disease is Ventilator Induced Lung Injury (VILI). When oxygen is delivered via mechanical ventilation, VILI can occur if the parenchyma

11

is over-stretched, resulting in higher shear stress that causes alveolar walls to rupture. Inflammation then occurs which can lead to edema or other cell trauma (DiRocco et al. 2006). Because it is extremely difficult to image the dynamic lung *in vivo*, it is not known how much airways and alveoli expand and contract during ventilation. It can be reasoned therefore that it is also not clear how airway pathology or alveolar function pathology relate to lung injury (Gatto & Fluck 2004). However, it is generally agreed that mechanical ventilation causes extracellular matrix remodeling and changes the biomechanical behavior of the lung. Changes in the extracellular matrix alter the mechanical forces on the cells, and redistribute how stress and strain are distributed in the parenchyma and alveolar walls (Pelosi & Rocco 2008). VILI is most dangerous when the alveoli actually begin to collapse. Atelectasis can occur in other disease states and as a result of lung injury. Once the alveoli are collapsed, the thin liquid lining or edema (if present) will hold the alveoli shut, requiring greater pressures to inflate them. Increasing the pressure delivered by a mechanical ventilator further increases the risk of alveolar rupture and collapse.

1.3.7 Conclusion of "What can go wrong with the lung?"

Research in lung mechanics thus requires understanding of some of the major ways the lung can become diseased or injured, so that relevant mathematical, laboratory and *in vivo* models can be developed and relevant questions addressed. From the perspective of Hubmayr (2002): When a clinician asks "How should I ventilate this patient?" the investigator should contemplate "How does an alveolus deform during a breath; what is the accompanying stress; how

do cells sense and respond to this stress; and finally can the cell and molecular responses of deformation be manipulated?" Because parenchymal compliance in the healthy lung is balanced to withstand cyclical strains and maximize gas exchange, any major alteration to that compliance, either stiffening as in pulmonary fibrosis or a slackening as in emphysema, or a spasm between the two as in asthma, will result in a disease state. And yet today, Tschumperlin et al. (2010) state that the role that stiffness (one aspect of lung compliance) plays in initiating, amplifying or prolonging these disease processes presents a fertile but as yet *unexplored* territory.

This discussion makes clear that every lung disease develops as the result of micromechanical changes. Lung injury and disease cannot be treated without adequate understanding of alveolar mechanics.

Section 1.4. *How* do scientists and researchers study the lung?

To obtain pressure-volume (PV) relationships for given patients, clinicians use a spirometer to measure volume and a pressure transducer to measure the difference between the tracheal (throat) and esophageal (thoracic) pressure. This pressure difference approximates the transpulmonary pressure, or the pressure difference between the outside and inside of the lung, and is usually thought of as the pressure required to inflate the lung (Mead 1973).

In the lab, a researcher could generate a PV curve using an animal model, an excised lung, or even a computer model. It is convenient to include generated PV

curves in published research so that clinicians can apply the findings. Studying and imaging the lung on a scale that resolves groups or individual alveoli is challenging. Animal lungs can be treated, fixed, excised and imaged, but sometimes these processes change inherent mechanical properties (Tschumperlin et al. 2010). However difficult, the lung has been imaged *in vivo* (Figure 5), most successfully and elegantly by Perlman & Bhattacharya (2007). This landmark study shows that there is a bright future for the development of visualization and measurement techniques of alveoli *in vivo*.
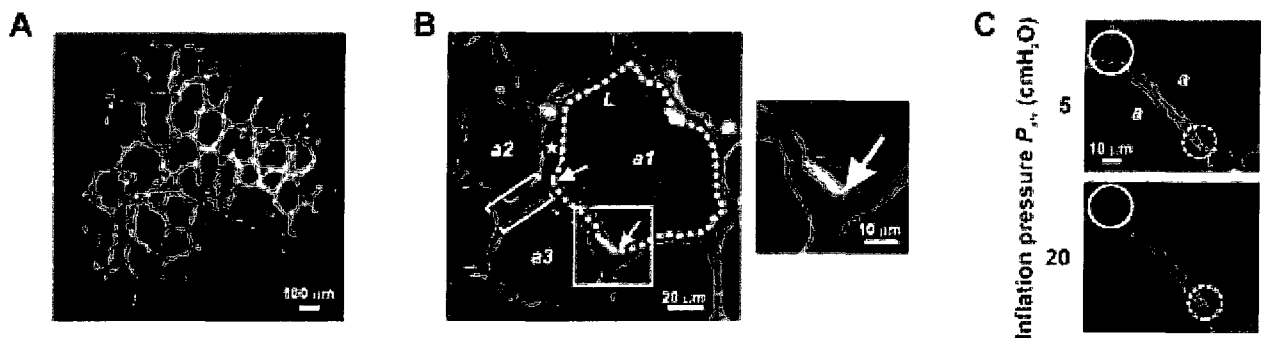
Figure 5: A) A low magnification image of a group of alveoli. B) A few alveoli and the marking technique and definitions used by the authors. C) Length change in a single alveolar wall imaged *in vivo* (from Perlman & Bhattacharya 2007).

As noted previously, the lung can be studied *in vivo*, *in vitro* and mathematically/ computationally. There is a wide variety of computational lung models. Some researchers have focused on the air flow in the airway tree, the inspiratory pump muscles, and even the dynamics of alveoli around and adjacent to an alveolar duct (Kitaoka et al. 1999, Ricci et al. 2002, Adler & Bates 2000). Regardless of the method of study, understanding of the lung is not yet complete.

Section 1.5. Contradictions in the lung research community

Researchers have proposed competing and contradictory mechanisms of lung inflation at the alveolar level, based on discordant descriptions and assessments of lung function (Gatto & Fluck 2004). In addition, conflicting *results* have been reported on the changes in the distribution of pleural pressures caused by alterations of chest shape (Vawter et al. 1975). Even today researchers disagree about how lung inflation affects alveoli, how the Law of Laplace is relevant in the lung, and the extent to which the thin film coats the alveoli, among other issues. These disagreements stem from the difficulty to excise and fix the lung to image it, and the fact that doing so changes thermo-chemical mechanical tissue properties. Even an *in vivo* measurement disrupts alveolar mechanics and is subject to resolution limitations. As an example of the sometimes extreme disagreement that exists in this community, the *Journal of Applied Physiology (JAP)* frequently publishes "Letters to the Editor" and "Controversies in Physiology" which are short discussions, often including rebuttals of lung mechanics researchers who have published articles in *JAP*. Both are forums in which contributing authors can debate each other's ideas and hypotheses (compare Hills 1999, Scarpelli & Hills 2000, and Gil 1983). In addition the following articles make conflicting statements about surface tension: Hoppin et al. (1998), Ingenito et al. (2005), West (2005), Hubmayr (2002), the Law of Laplace: West (2005), Prange (2003), Fung (1975a), Hamm et al. (1996), alveolar wetting: Hills (1999), Scarpelli & Hills (2000), Gil (1983), Gatto & Fluck (2004), and edema distribution: Bachofen et al. (1993).

Section 1.6. Motivation and method

Motivated by the contention between lung researchers and the need for improved fundamental understanding of alveolar mechanics, we developed and investigated a mathematical model of an alveolar network that includes pressure, surface tension, geometrical considerations, and material behavior. Our model is close to that of Suki & Bates (2008) and Flicker and Lee (1974), but we augment the simplified spring model by including the effect of *both* pressure and surface tension. Pressure is the essential driving force of every inhale and exhale and must be included in a lung mechanics model for completeness. In addition, we specifically seek to understand how surface tension impacts alveolar mechanics.

We have developed two related models to study alveolar mechanics: An analytical model of a small network of alveoli and a computational model (using Matlab) of an arbitrary sized network. Our primary focus is on static force balances in these model alveolar networks. Although the lung is a dynamic organ, static balances are necessary to build the foundation for dynamic models.

Because this model is an abstraction of an alveolar network, retaining only essential physical and geometrical ingredients, results of this research may be applicable to other systems. Any material, biological to industrial, composed of unit cells (hexagonal cells would be most similar) could be modeled using a similar approach.

Our overarching goal is to understand the relationship between surface tension, geometry, and material properties as manifested in a model alveolar network. More specifically, we would like to know how the PV curve, in our case the pressure-area (PA) curve, is impacted by these factors. We aim to isolate the impacts of these various factors and ultimately incorporate work of colleagues (James Melfi and others) who have modeled alveolar septal dynamics.

CHAPTER 2.

Problem Formulation

Section 2.1. Physiological model justification

2.1.1 Geometrical considerations

In this investigation, we model the geometry of a group of alveoli as a two-dimensional (2D) hexagonal network. To justify this choice as an appropriate first step in a lung model, see Table 4, which includes pictures, artistic renditions, casts and SEM images of the lung from organ to cell for intuition regarding scale and physiological form. Previous investigators have modeled the lung as either an open (Mead 1973) or closed system (Haber 2000). We opted to follow the latter approach so that we could study the conformations of a pressurized network.
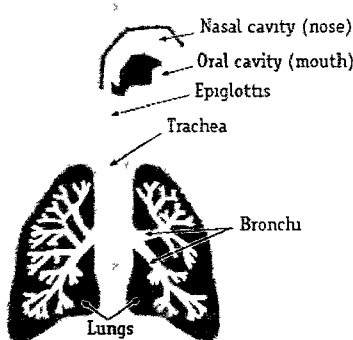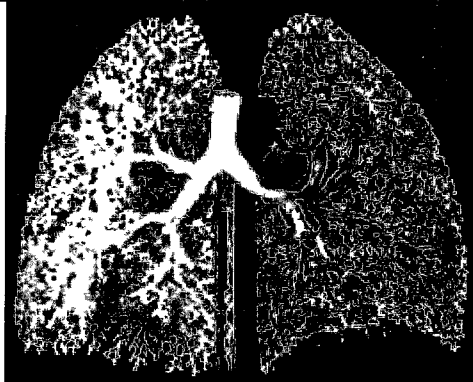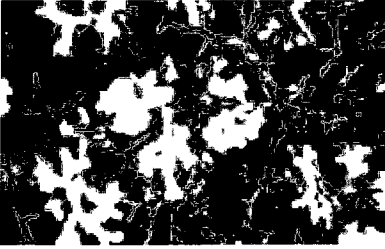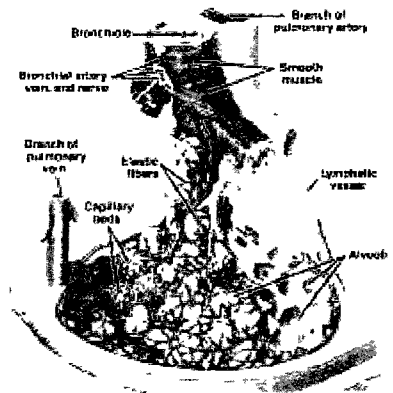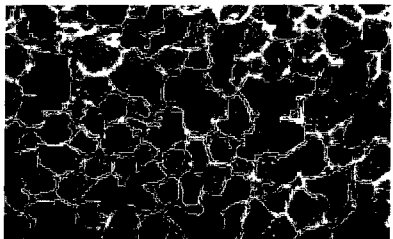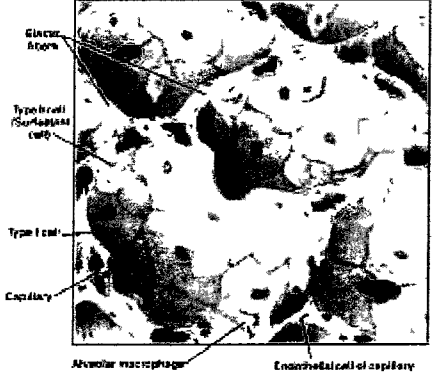
Organ The trachea leads from the nose and mouth to the bronchi which bifurcate and terminate at the alveoli. The right picture is a resin cast of a human lung.	 Nasal cavity (nose) Oral cavity (mouth) Epiglottis Trachea Bronchu Lungs	 Red and blue vessels carry oxygenated and deoxygenated blood, airways are yellow.
Alveolar clusters The airways terminate in alveolar clusters that are the site of gas exchange and are highly intervasculated.		
Septal walls All alveoli share their walls with their neighbors. The walls are slightly wider than a blood cell. The left SEM image shows a roughly hexagonal network.		

Table 4: The lung from organ to cell. As the reader progresses from the top left image to the bottom right image the scale decreases from about 1 meter across a human rib cage to 100 microns across a single alveoli, with the septal walls being about 10 microns thick (from European Lung Foundation 2011, Bautista et al. 2011).

2.1.2 Springs used as tissue models in the literature

As can be seen in the SEM image in Table 4, a hexagonal network model is a reasonable (albeit abstracted) representation of a cross-section of the lung. Of course, for pressure to impact alveolar septa, the septal faces must be 2D (i.e. generally planar surfaces). In our 2D network model, one edge of each septal face is assumed to be very long (as in a honeycomb-like structure) and every relevant input is divided by "width" to create one-dimensional elements that we term "springs". This terminology should not be interpreted literally; indeed, it is hard to conceptualize how pressure would impact a spring network. The idea is that we are representing membrane behavior with springs but maintaining the pressure effect.

In fact, alveolar walls have commonly been modeled as springs in the field of pulmonary micromechanics. For instance, Mead, Takishima, and Leith in 1970 designed a spring table with interconnected springs in a hexagonal pattern and the outermost springs attached to weights. They could modify the shape of the inner-most hexagon and then visually assess the consequent changes in their 36 hexagon network (see Figure 6).
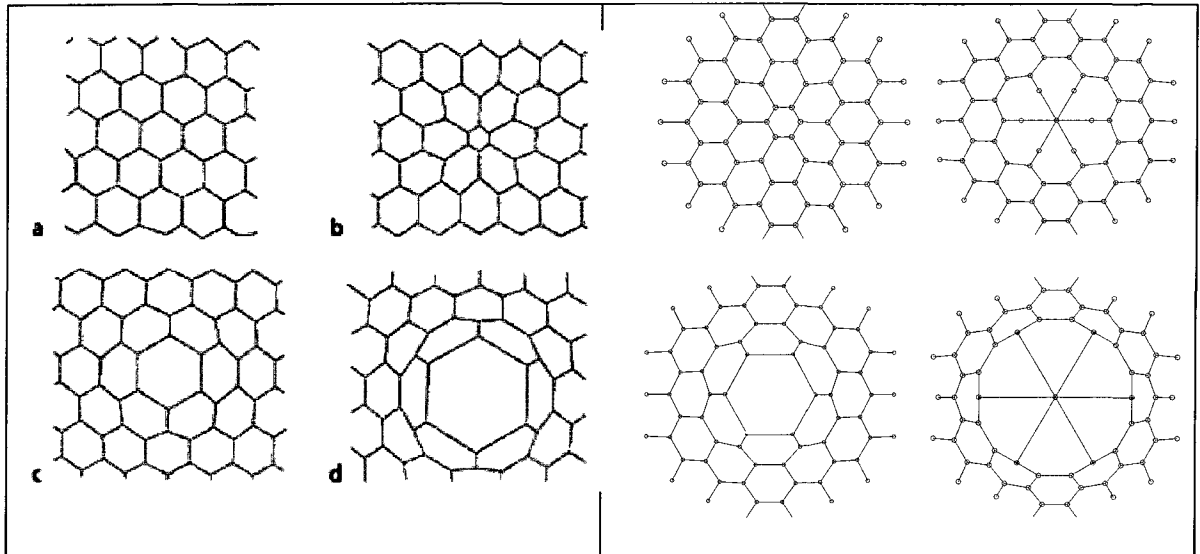
Figure 6: From Mead, Takishima and Leith 1970 On the left is Figure 15 from Mead et. al paper. On the right is a sample of our computational results for visual comparison.

Another widely cited report was authored by Cavalcante et al. (2005). Regarding their numerical model, they state that "The elastic behavior of the tissue sheet was modeled by using a two dimensional network of nonlinearly elastic springs joined by pin joints. Each spring represented the combined mechanical behavior of elastin and collagen fibers within the alveolar wall ... Where k is the linear spring constant and b is the nonlinear spring constant." This report compared numerical simulations of nonlinear springs in a hexagonal network with *in vivo* measurements of alveolar septa.

Lastly, we cite the work of Hung et al. (2010) who modeled the sclera (or outer-most membrane) of the eye-ball with a network of interconnected springs (see Figure 7). These authors modeled eye tissue mechanics with Hooke's Law and treated the system as time dependent (dynamic) to capture changes in viscoelasticity of the nonlinear spring network.

21

Linked spring model of
the scleral matrix

Free body diagram of an
individual node
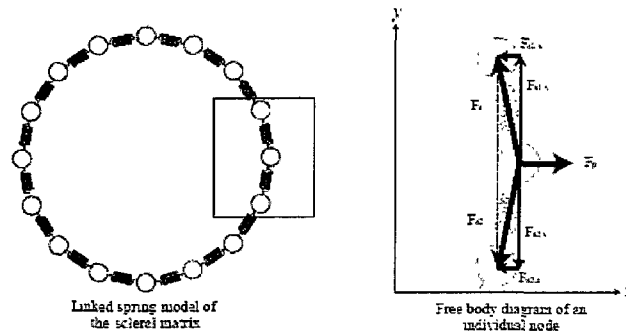
Figure 7: Spring model of the sclera (from Hung et al. 2010).

In addition to the research cited above, numerous other articles incorporate

spring models of mechanics including Bates (2007), Faffe & Zin (2009), Suki &

Bates (2008), Bachofen et al. (1993), Fung & Sobin (1972), Adler & Bates

(2000).

2.1.3 Surface tension discussion

Although the extent to which a thin film of fluid lines the lung (see Introduction), it

is agreed by researchers, that there is some liquid lining the lung. We have

chosen to approximate this lining, as a thin film of fluid that forms pools in the

corners of alveoli and resists inflation. In this project we have not defined the

volume or constituents of the fluid, but we have assumed that it makes a zero

contact angle with the septa it lines; thus the surface tension force acts parallel to

the resistive spring force. Figure 8 shows a simple drawing of how we have

assumed the thin film lining the lung to pool in alveolar corners. The blue arrows

are the "border" of the pool and represent the surface tension force that is

multiplied by the width of the septal membrane and is parallel to the resisting

22

"spring" force of the membrane. To clarify, if we were to express the force due to surface tension on this particular membrane it would be γb.
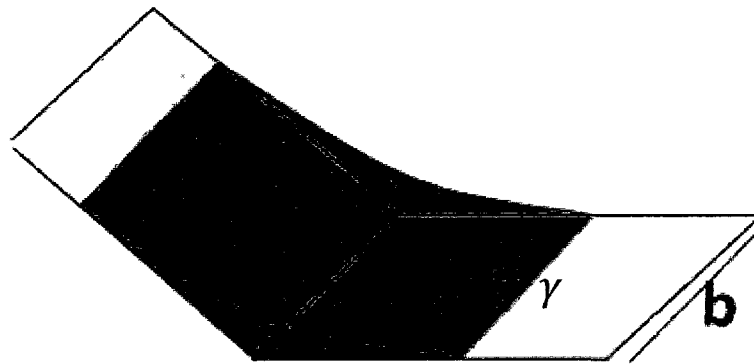
Figure 8: 2D conceptualization of liquid lining pools in the corner of an alveoli.

2.1.4 Pressure discussion

The lung is a remarkably efficient organ; the pressure required to move gas through the airways is very small, about 2 cm of water to move air about 1 liter/second (West 2005). Physiologists have many names and many ways to describe pressure. For our purposes we will familiarize the reader with the most commonly used terminology. (Usually, when referring to the lung pressure has units of cm H_2O and volume is measured in liters.)
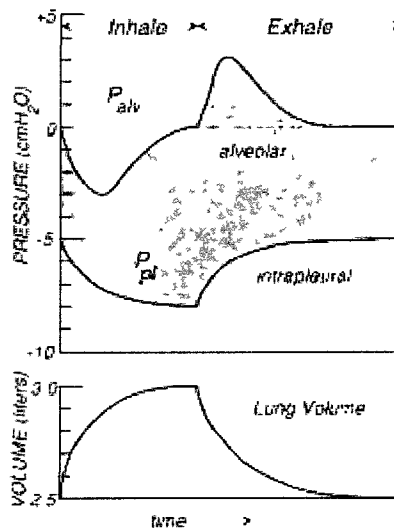
Figure 9: Changes in lung volume, alveolar pressure, pleural pressure and transpulmonary pressure during normal breathing (from Brown 2010).

Alveolar pressure: Alveolar pressure (Palv) in Figure 9 is the pressure inside

the alveoli. When the mouth and throat is open (specifically the glottis) and no air

is flowing into or out of the lungs, the pressure in all parts of the respiratory tree,

all the way to the alveoli, is equal to atmospheric pressure, which is considered

to be the primary reference pressure (Guyton & Hall 1996).

Pleural pressure: (First recall that there are no attachments between the lung

and the wall of the rib cage. Therefore the lungs are held to the thoracic wall as if

glued there, except they can move freely as the chest expands and contracts.)

Pleural pressure (Ppl in Figure 9) is the pressure of the fluid in the narrow space

between the lung pleura and the thoracic wall pleura. There is normally a slight

suction, which means a slightly negative pressure about -5 cm H_2O. Facilitated by

suction, the rib cage "pulls" on the surface of the lung pleura causing it to expand

and the pleural pressure decreases to about -8 cm H_2O (Guyton & Hall 1996).

24

Transpulmonary pressure: Transpulmonary pressure is the difference between the alveolar pressure and the pleural pressure (the shaded region in Figure 9). Essentially it is the measure of pressure required to keep the lung patent (Guyton & Hall 1996).

In order for air to flow into the lung, the pressure in the alveoli must fall to a value slightly below atmospheric pressure, about -1 cm H_2O. During expiration the opposite changes occur, and alveolar pressure rises to about +1 cm H_2O (Guyton & Hall 1996). PV curves usually plot volume change (ordinate) versus transpulmonary pressure (abscissa) but it is not uncommon to see volume versus pleural pressure or alveolar pressure.

Very closely related to the PV curve is the lung compliance curve. Just as the name suggests, lung compliance is a measure of how much the lung expands for given changes in transpulmonary pressure. In a healthy lung at rest, the lung expands by 200 ml for a transpulmonary pressure increase of 1 cm H_2O (Guyton & Hall 1996). Because lung tissue is viscoelastic the PV curve (or stress strain $\sigma - \epsilon$ curve) will always be hysteretically shaped. Drawings of common PV and compliance curves are shown below.
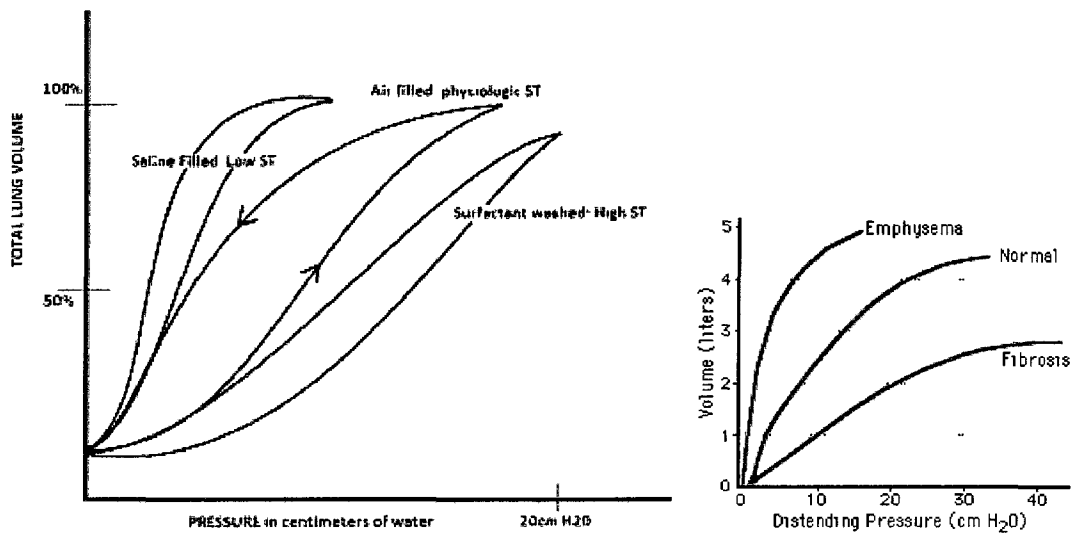
Figure 10: Three PV curves of the lung with total lung volume versus pressure in cm H20. The arrows on the center curves indicate inspiration ("Up" arrow) and expiration ("Down" arrow).The saline filled lung requires lower pressure to fill the lungs to physiologic volume. The air filled lung, by area inside PV curve, requires the greatest work to fill the lung. The surfactant washed lung has no active surfactant, so the liquid lining in the lung acts on the alveolar septa with greater surface tension force. This leads to alveolar collapse, widening of alveolar ducts; septa are "sucked" together to widen the ducts even more.

Figure 11: Compliance curves showing disease states from (Johns Hopkin's School of Medicine 1995)

As can be seen in Figure 10 and Figure 11, the PV curve can change shape depending on what is happening inside the lung, and can be used as an initial screening or diagnostic tool, or it can be used by non clinical researchers as a dynamic picture of lung mechanics.

Hysteretic PV curves can be generated from measurements on graphs like Figure 9. Although not apparent by inspection, the PV curve and Figure 9, plot the same data in different ways. For this discussion and plots see APPENDIX A. Also in this appendix are references about how pressure and volume are measured in humans in a clinical setting.

Section 2.2. Framing the force balance

As noted above, using springs to model biological tissue is accepted in the field of lung mechanics research and also other biomechanical fields. Using springs enables researchers to model highly complex tissues with simple force balances. In our model, we use linearly elastic springs, meaning that they have a one to one relationship between the force in each spring and the amount it is stretched. This relationship is known as Hooke's Law:

$$F = K\Delta x,$$

where F is the force, K is the spring constant, and Δx is the change in length of the spring from its unstretched length. Of course, a more accurate model of an alveolar wall would be a viscoelastic or nonlinearly elastic spring, however using a linearly elastic spring network is an appropriate first step.

Also we have assumed that surface tension has a zero contact angle along the septal "springs", and that it acts parallel to the resistive spring force. So an inflation pressure is resisted by the spring force and the force due to surface tension. This figure illustrates a sample free body diagram with surface tension and described in detail in Section 3.3.
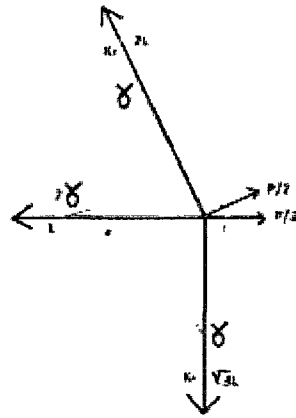
Figure 12: 2D conceptualization of surface tension.

In addition to spring and surface tension forces, we impose a pressure difference to deform the network. Our approach is similar to that of Flicker and Lee (1974). As can be seen in Figure 13, these researchers derived a force balance for a roughly hexagonal, 2D network with an imposed pressure (denoted as P_L).
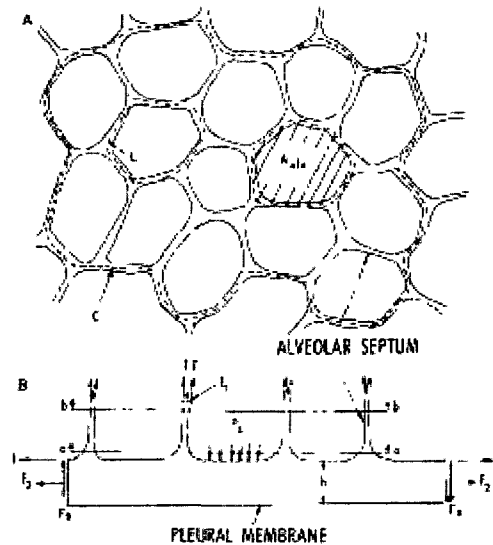
Figure 13: Roughly hexagonal network illustrated by Flicker & Lee 1974, with corresponding side view below.

28

A force balance of static alveolar mechanics must include a pressure difference and a sum of forces over some area in two dimensions. To illustrate the analysis, consider a force balance on a network consisting of seven complete hexagons (Figure 14).
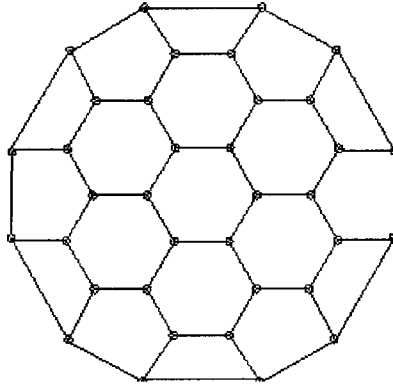
Figure 14: Seven hexagon network.

The internal, inflating pressure acts outward in all alveoli, just as if each alveolus had its own pressure source. Calculating a force balance on an internal node, the pressure on all three adjacent springs is equalized by an opposing pressure from the neighboring alveoli. Hence, for a homogeneous pressure distribution, pressure only makes a *net* contribution to the force balance on the pleural nodes since there is no (relative) pressure acting outside the network. In addition to developing a computational model by imposing a force balance for each node, internal and pleural, we also have obtained an analytical pressure area (PA) solution in the case of a seven hexagon network possessing a high degree of symmetry. For the seven hexagon network, Figure 15 shows a pleural node free body diagram, (see Section 3.3 for complete explanation of forces and equations).
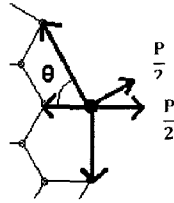
Figure 15: Pleural node free body diagram.

2.2.1 Model assumptions

In order to model this complex system, certain assumptions must be made. Depending on the goals and uses of the model, different assumptions may be relevant. For our specific model, applicable assumptions are listed in Table 5.

Physiological Characteristic	Assumption	Consequence
Alveolar shape	Regular Hexagons	Lung is highly heterogeneous in shape and parenchymal tissue properties, mechanics may or may not be comparable
Alveolar Dimension	2 Dimensional	2D extrapolation of 3D structure not complete, may omit crucial mechanical details
Pressure	Internal pressure	Lung is not inflated from the inside, it is expanded by the external action of muscles
Pleural Surface	Planar	The surface of the lung encompasses the entire lung not a small group of alveoli and is curved not planar
Septal material properties	Linear springs	Does not capture time dependence of viscoelastic or nonlinearly elastic tissue
Force Balance	2D lattice in plane	Pressure acts uniformly along each element
Breathing	Static	Static force balance does not capture any time dependent aspects of alveolar mechanics which is inherently dynamic

Table 5: Assumptions made in computational model and input parameters.

As is clear in this table, our model captures only static (i.e. equilibrium) behavior: there is no time dependence in our equations or variables. This is deemed to be necessary and a natural first step toward developing a dynamic model.

2.2.2 Nondimensionalization

To most conveniently assess the relative magnitudes of different physical, material, and geometrical effects, it is helpful to non-dimensionalize the various terms arising in the nodal force balance. First we define constituent material properties: a table listing these properties is shown below.

Physiological Parameter	Variable	Computational Input	Source
Transpulmonary pressure about 5 cm/H_2O	P	490 N/m^2	West 2005
Unstretched length of alveolar septa	L_0	$50e^{-6}$ m	Perlman & Bhattacharya 2007
Elastic modulus of alveolar septa	E	5000 N/m^2	Suki et al. 2005
Thickness of alveolar septa is slightly thicker than a blood cell (8um)	t	$10e^{-6}$ m	West 2005
Surface tension in the lung varies with area from about 5 to 60 dynes/cm	γ	0.06 N/m	West 2005

Table 6: Physiological values of constituent material properties.

Using Table 6 as a reference, we will now derive non-dimensional force balance equations and non-dimensional parameters. Starred terms are dimensional. As defined in Equation 1, strain ϵ_s is a change in length of a septa over original length. The force in a single septa (spring) F_s follows Hooke's Law in Equation 2. F_s acting on a septa with width b and thickness t is defined as stress σ_s. Stress can also be defined as elastic modulus E of a membrane multiplied by the strain (Equation 5). Using these relationships we derive a non-dimensional force balance and parameters:

31

$$\epsilon_s^* = \frac{L^* - L_0^*}{L_0^*}$$

Equation 1

$$F_s^* = K^*(L^* - L_0^*)$$

Equation 2

$$\sigma_s^* = \frac{F_s^*}{b^* t^*}$$

Equation 3

$$\sigma_s^* = E^* \epsilon_s^* = E^* \frac{L^* - L_0^*}{L_0^*}$$

Equation 4

$$\frac{F_s^*}{b^* t^*} = E^* \frac{L^* - L_0^*}{L_0^*}$$

Equation 5

$$\frac{K^*(L^* - L_0^*)}{b^* t^*} = \frac{E^*(L^* - L_0^*)}{L_0^*}$$

Equation 6

$$K^* = \frac{E^* b^* t^*}{L_0^*}$$

Equation 7

Note, although we are stretching the springs, we are assuming the thickness of the spring does not change. We can now use these relationships in our typical force equations, which will be derived in detail in Section 3.1 and are of the form:

$$\sum F_s^* = K^*(L^* - L_0^*) \pm P^* L^* b^* \pm \gamma b^*.$$

Equation 8

Dividing each term by b, the width of the membrane, we obtain

$$\sum \frac{F_s^*}{b^*} = \frac{E^* t^*}{L_0^*}(L^* - L_0^*) \pm P^* L^* \pm \gamma^*$$

Equation 9

Further division by L_0 and the spring constant per unit width $K_0^* = \frac{E_0^* t_0^*}{L_0^*}$ yields

$$\sum \frac{F_s^*}{b^* K_0^* L_0^*} = \frac{E^* t^*}{L_0^* K_0^* L_0^*}(L^* - L_0^*) \pm \frac{P^* L^*}{K_0^* L_0^*} \pm \frac{\gamma^*}{K_0^* L_0^*}.$$

Equation 10

Also note, $K_i^* = \frac{E^* t^*}{L^*}$.

Thus the non-dimensional, generic force equation becomes:

32

Equation 11

$$\sum F = K_i(L-1) \pm PL \pm \gamma,$$

where the non-dimensional parameters are:

$$F = \frac{F_s^*}{b^* K_0^* L_0^*}, \quad K_i = \frac{K_i^*}{K_0^*}, \quad K_B = \frac{K_B^*}{K_i^*}, \quad K_s = \frac{K_s^*}{K_i^*}, \quad L = \frac{L^*}{L_0^*}, \quad P = \frac{P^*}{K_0^*}, \quad \gamma = \frac{\gamma^*}{K_0^* L_0^*}.$$

Using values from Table 6, an order of magnitude calculation gives:

$$P^* = \frac{490 \frac{N}{m^2}}{1000 \frac{N}{m^2}} = 0.49$$

$$\gamma^* = \frac{0.06 \frac{N}{m}}{1000 \frac{N}{m^2} * 50 e^{-6}\ m} = 1.2.$$

When assessing these values in the force balance equation, we note that the magnitudes of the non-dimensional pressure and surface tension are comparable. From now on, these non-dimensionalized parameters are referred to as their "un-starred" equivalents (e.g. $F^* = F$), unless specifically noted otherwise.

Section 2.3. Stretching versus bending

As forces are applied to the springs, we consider only that they stretch and not bend. Mechanically, membranes and springs have no resistance to bending, but they do resist stretching. Realistically, alveolar septa may have resistance to bending in two or three dimensions. We could model this by adding a rotational resistance around each node, so that the springs would resist tension as well as rotational bending around a node. Our current model, however does not include bending resistance.

Section 2.4. Statics and dynamics

2.4.1 Statics

As noted previously, we consider only (quasi-) equilibrium conformations of our network model. We calculate our network force balance by accounting for the forces on each node. To calculate pressure forces, we assign one-half the pressure on a given "septa" to each of the two nodes to which that septa is attached. Proceeding in this way we obtain a system of *nonlinear* algebraic equations for the unknown (deformed) positions of each node. But there seems to be a contradiction here: "If the springs are linear springs and the equations are linear how can this be a nonlinear system?" The answer is that the equations are, in fact, not linear, because the spring forces are of the form

$$F = K\Delta x \frac{\Delta x}{\sqrt{x^2 + y^2}}.$$

Equation 12: Hooke's Law and unit vector direction

In Equation 12 we recognize Hooke's Law with an additional term: In order to describe the direction of the spring force we must also have a directional unit vector which can be described in the form of sines and cosines or in vector notation as it is in Equation 12. It can now be seen, with this general example, that our system of equations is nonlinear when expressed in terms of the unknown (x and y) coordinate locations of the nodes. To solve this nonlinear system, we use an iterative Newton-Raphson method in Matlab.

2.4.2 Dynamics

Once we have validated the computational models with an analytical solution, we can move beyond analytical solution methods by increasing network size,

34

introducing viscoelastic material properties and explore the thin film's impact in a dynamic cycling simulation. One goal would be to increase the level of complexity of the model to approach the complexity of the lung and capture realistic alveolar mechanics. Another goal would be to incorporate computational work of colleagues who are solving a thin film equation for a corner in a regular hexagon in a dynamic state. This approach would yield systems of nonlinear algebraic equations to systems of partial differential equations that would more fully capture alveolar mechanics.

CHAPTER 3.

Analytical Predictions

The motivation for deriving analytical solutions for a network force balance was two-fold. First, we wanted to have an independently derived solution to validate the computational solution. Second, the analytical solution makes clear the *parametric* dependencies of outputs.

Section 3.1. Method

Throughout this text we will reference two types of analytical predictions: exact analytical solutions and approximate analytical solutions. In this chapter we will frame how we derived the exact analytical solutions. The next chapter will refer to estimated solutions for larger networks.

Exact analytical solutions were derived only for the single and seven hexagon networks due to the additional degree of freedom needed for larger networks (as will be described in Section 3.4 of this chapter). These expressions came directly from the force balances of these networks as introduced in Section 2.2.

Section 3.2. Single hexagon network

To verify that the code for a single hexagon (with 6 nodal force balances) converged to an equilibrium solution, we compared the computational stretched length of one spring to the exact analytical solution derived from the force

balance, (where all lengths are the same in a hexagonal equilibrium configuration). The exact analytical solution was calculated using the following (non-dimensional) equation:

$$L = \frac{K_i}{K_i - \frac{\sqrt{3}}{2}P}$$

We used non-physiological, dimensional values to test the single hexagon, because the solution would be valid for a zero solution to the force balance. The single hexagon had sides with unstretched length of 1 coordinate unit, pressure and the spring constant were also chosen to be on a comparable order. The relative error for the single hexagon below 10^{-12}%, indicating a precise correspondence for the solution of the single hexagon. After this first check of code validity, we were satisfied to increase complexity to a network of seven hexagons.

Section 3.3. Seven hexagon network

To obtain an analytical solution for the seven hexagon network, we sought a deformed conformation that maintained a high degree of symmetry. Specifically, this network can be divided into twelve symmetric wedges.

37
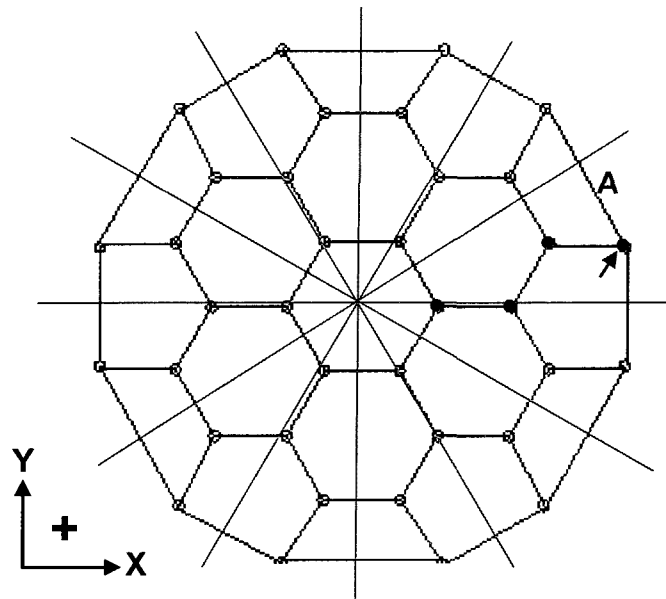
Figure 16: Seven hexagon network can be divided into twelve symmetric wedges.

Consider the wedge labeled "A" in Figure 16. Inside wedge A, there are four nodes, shown in bold. Working out the force balance, including pressure but not surface tension, for each node, we find that the three internal nodes trivially satisfy the X and Y force balances. For the pleural node (bold node with arrow), however, the non-dimensional force equations are not trivially zero. They are:

$$\sum F_x = 0: PL = \frac{K_i}{\sqrt{3}}(L - 1) + \frac{K_B}{2\sqrt{3}}(2L - 1),$$

Equation 14

$$\sum F_y = 0: PL = 2K_s(\sqrt{3}L - 1) - \sqrt{3}\,K_B(2L - 1),$$

Equation 15

with

$$K_B = \frac{2}{7}(1 + \sqrt{3})K_i,$$

$$K_S = \frac{1}{6}(3 + 2\sqrt{3})K_i,$$

Note that K_i is prescribed as is P (and L_0 in dimensional form). Thus, the only unknown in these *two* equations is L, the stretched length. To obtain a unique solution, K_s and K_B must be chosen according to Equation 16 and Equation 17, for the stretched length (i.e. the equations become redundant), we also require that these material properties are independent of stretched length L.

A more physical model, such as Mead, Takishima, and Leith's (1970), would have equal spring constants and initial spring lengths to correspond with the chosen equilibrium shape. Computationally however, we found that this set-up would not have an equilibrium solution for any non-zero pressure.

In this way, we obtain one equation where we prescribe the pressure, unstretched length, and spring constants and which yields the stretched length. Furthermore, since we have determined the pleural node is the only node that has a non-trivial force balance in the wedge and the wedge is the network's unit of symmetry, this one equation governs the force balance for the *entire* network: for a given input pressure, the new stretched length for all the springs in the network can be determined.

In addition to varying the spring constants and pressure, we can also vary the magnitude of the surface tension γ. For a dry network, γ is set to zero, but for wet networks $\gamma > 0$. As a rule of thumb, γ must be of a comparable order as the pressure and spring constants for surface tension to play a role. Figure 17 shows a free body diagram (FBD) of a pleural node with surface tension included and the corresponding (non-dimensional) force balances are given in Equation 18 and Equation 19.
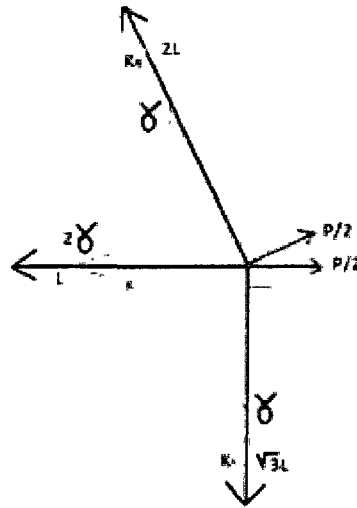
Figure 17: Free body diagram of pleural node with surface tension γ. Equation 18 and Equation 19 were derived from this FBD. Note the surface tension force on the two pleural elements is γ while on the internal element is 2γ.

$$\sum F_x = 0: PL = \frac{K_i}{\sqrt{3}}(L-1) + \frac{K_B}{2\sqrt{3}}(2L-1) + \gamma\left(\frac{5}{2\sqrt{3}}\right)$$

Equation 18

$$\sum F_y = 0: PL = 2K_s(\sqrt{3}L - 1) - \sqrt{3}\,K_B(2L-1) + \gamma(2 - \sqrt{3})$$

Equation 19

with

$$K_s = \frac{\frac{1}{2}K_i + (2\sqrt{3} - \frac{11}{2})\gamma}{2\sqrt{3} - 3}$$

Equation 20

40

$$K_B = \frac{6K_s - K_i}{7}$$
Equation 21

As above, K's, P, L0 are all prescribed and the only unknown for these redundant

two equations is stretched length L. Specifically, we rearranged Equation 19, to

get an (non-dimensional) expression for stretched length L to be

$$L = \frac{\left(2K_s - \sqrt{3}K_B\right) - \gamma(2 - \sqrt{3})}{2\sqrt{3}(K_s - K_B) - P}.$$

As will be seen in the next chapter, the average percent error between the

computational and analytical solution for the seven hexagon network is 1%,

which is greater than the computational/ analytical error for the single hexagon,

but we continued with the model do to its convergence properties, force balance

satisfaction, and small error most likely due to round off error.

Section 3.4. Larger networks

Just as a single element has specific material properties, so can an entire

network. In their book, *Cellular Solids: Structure and Properties*, Gibson and

Ashby describe how to find effective properties of honeycomb networks in

Chapter 4. Because this chapter was written from a mechanics of manufacturing

perspective, they do not derive any relationships for inflated honey-comb

networks.

We have chosen a very specific geometry for these networks: the sides of the

networks are prescribed as flat and the flat edges extend as network size

increases.
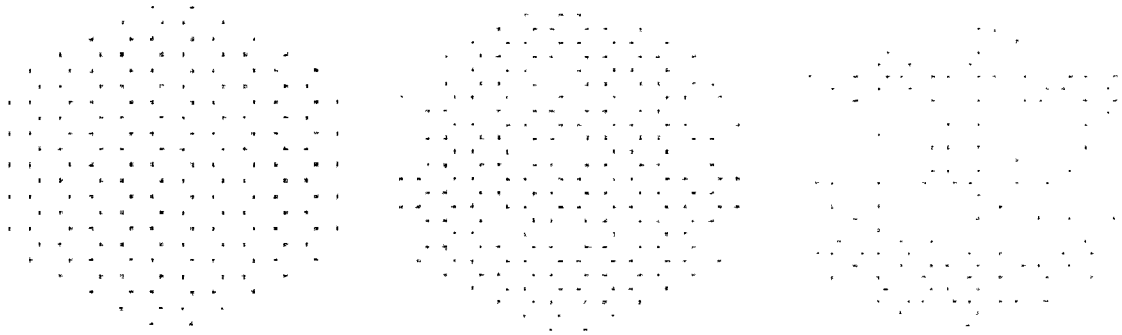
Figure 18: Increasing network size. With this prescribed geometry, the external geometry remains as the inside is filled with more and more hexagons.

To attempt to find an analytical pressure-length relationship for these larger networks, we again divided the network into symmetric wedges. The force balance from the seven hexagon network was included in each larger network. For each additional annular "ring" of hexagons, another equation became relevant. The vertical portions of the networks had multiple nodes that accounted for an outward directed pressure and inward directed spring resistive force. However, herein lies the barrier to finding an analytical force balance for larger networks. For every second size increase, a new equation describing the force on a vertical node is added. This means that every new equation brings with it a new degree of freedom that is required to solve three equations for two unknowns. So as the number of hexagons increases, the necessary degrees of freedom also increases, preventing us from deriving a size dependent force balance. Bear in mind however, for a different geometry this problem may not be encountered. For instance, if a rounder external geometry (Figure 19) was approached highly symmetric solutions for increasing number of hexagons may be possible.
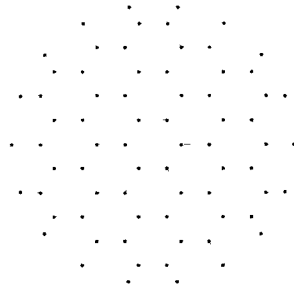
Figure 19: Rounder network.

Although the geometry we have chosen has prevented us from obtaining highly symmetric analytical solutions for larger networks, we have been able to derive analytical *approximations* for the effective modulus of large networks. First, we determined the effective (network-wide) force of an inflated network, assuming regular hexagonal geometry.
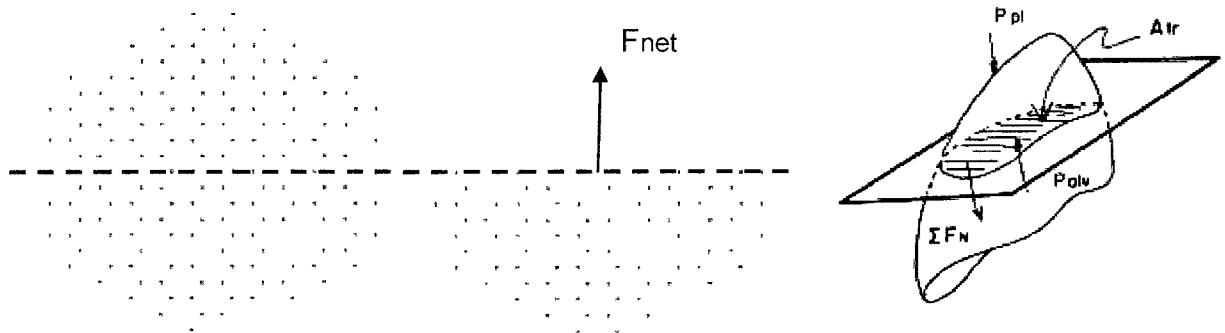
Figure 20: A cut through a network to find effective properties. The drawing on the right is from (Mead et al. 1970) and shows how effective force (F_N) was approximated with a similar method.

To find the effective force F_{net} we define network characteristics, e.g. network diameter, the number of hexagons in the network and the number of hexagons adjacent to the cut. We have defined F_{net} to be equal to a coefficient of effective force multiplied by the force in a single spring element as follows:

43

$$F_{net}^* = P^*D^* = C_F F_s^* \cos\theta.$$ <div style="text-align: right">**Equation 22**</div>

The pressure force exposed over the diameter of the network is opposed by the

forces in all of the cut springs. The following network characteristics are useful in

calculating effective properties:

Rings around center (rg)	Total Hexagons (N)	Hexagons across cut	Force Coefficient (C_F)
0	1	1	2
1	7	3	4
2	19	5	6
3	37	7	8
4	61	9	10
5	91	11	12
Relationships:	$N = 1 + 6\sum\limits_{n=0}^{rg} n$		$C_F = 2(rg + 1)$

Table 7: Network relationships.

Using reasoning parallel to that in Section 2.2.2, we can also express network

strain and effective properties. The variables used below are as follows: stress σ_s

in a single spring, elastic modulus E, stretched length L, width b, thickness t,

diameter of the network D_{net} (as a horizontal measurement from left to right),

coefficient in the effective force equation C_F, stress in the network σ_{net}, resultant

force of cutting the network in half F$_{net}$, and force in a single spring F$_s$. Equation

23 and Equation 24 are *dimensional* expressions for the stress in a single spring,

and Equation 25 is a *dimensional* expression for a spring constant:

$$\sigma_s^* = E^* \frac{\Delta L^*}{L_0^*},$$ <div style="text-align: right">**Equation 23**</div>

$$\sigma_s^* = \frac{F_s^*}{b^* t^*},$$ <div style="text-align: right">**Equation 24**</div>

$$K^* = \frac{E^* b^* t^*}{L_0^*}.$$

Next, we give an expression for the diameter of a network in terms of the stretched length of a single spring and C_F. We claim that network strain and (single) spring strain are equal according to Equation 28. To show this we use a derived expression for D_{net} and an approximate relationship between spring and network strain.

$$D_{net}^* = L^*(\frac{3}{2}C_F - 1)$$

$$\epsilon_s = \frac{\Delta L^*}{L_0^*} \sim \epsilon_{net} = \frac{\Delta D^*}{D_0^*}$$

Equation 27 holds by the following:

$$\frac{\Delta D^*}{D_0^*} = \frac{D_{net}^* - D_0^*}{D_0^*} = \frac{\left(\frac{3}{2}C_F - 1\right)(L^* - L_0^*)}{\left(\frac{3}{2}C_F - 1\right)L_0^*} = \frac{L^* - L_0^*}{L_0^*} = \frac{\Delta L^*}{L_0^*}.$$

With these equations we derive an effective modulus relationship.

$$C_F = \frac{2}{3}\left(\frac{D_{net}^*}{L^*} + 1\right)$$

$$F_{net}^* = \frac{\sqrt{3}}{3}\left(\frac{D_{net}^*}{L^*} + 1\right)F_s^*$$

$$F_s^* = \frac{E^* b^* t^* \Delta L^*}{L_0^*} + 2\gamma^* b^*$$

$$F_{net}^* = \frac{\sqrt{3}}{3}\left(\frac{D_{net}^*}{L^*} + 1\right)\left[\frac{E^* b^* t^* \Delta L^*}{L_0^*} + 2\gamma^* b^*\right].$$

Now we have an expression for the total net force of a horizontally sliced network under strain imposed by inflation pressure. Recall, Equation 23 and Equation 24

are the stresses in a single spring. Equation 33 expresses the (dimensional) stress analog for a network in terms of the network size and initial parameters.

$$\frac{P^* D^* b^*}{b^* D_0^*} = \sigma_{net}^* = \frac{F_{net}^*}{b^* D_0^*} = \frac{\sqrt{3}}{3} \frac{E^* t^*}{D_0^*} \left(\frac{D_{net}^*}{L^*} + 1 \right) \frac{\Delta D^*}{D_0^*} + \frac{2\gamma^*}{D_0^*}$$
<div align="right">**Equation 33**</div>

$$P = \frac{\sqrt{3}}{2} \left(\frac{C_F}{\frac{3}{2} C_F - 1} \right) \frac{1}{L^*/L_0^*} \left[K_i^* \left(\frac{L^*}{L_0^*} - 1 \right) + \frac{2\gamma^*}{L_0^*} \right]$$
<div align="right">**Equation 34: Dimensional solution for L**</div>

$$P = \frac{\sqrt{3}}{2} \left(\frac{C_F}{\frac{3}{2} C_F - 1} \right) \frac{1}{L} [K_i(L - 1) + 2\gamma]$$
<div align="right">**Equation 35: Non-dimensional form**</div>

We use this equation to *predict* the solution for larger networks (that have no analytical solution) in Section 4.4. In addition, we have found a simple method to generate larger networks which is described in APPENDIX C.

CHAPTER 4.

Computational Results

Section 4.1. Numerical algorithm

To arrive at solutions of larger networks, we calculated nodal force balances for each node in the network. To solve the resulting system of nonlinear algebraic equations we used the Newton-Raphson (NR) method. Our approach is similar to that of Adler & Bates (2000), who developed a computational model of an airway surrounded by concentric rings of alveoli (which they termed an "alveolar ring model"). These researchers minimized the potential energy functional with a nonlinear least squares minimization. We go one step further: rather than minimizing the energy functional, we force the residual net force on each node to vanish (to within some prescribed tolerance).
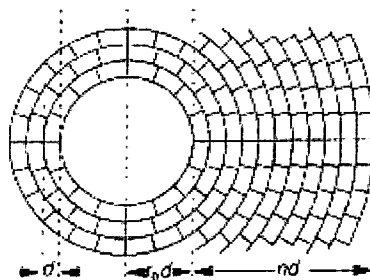
Figure 21: Alveolar ring model (from Adler & Bates 2000).

Our computational algorithm consists of three nested functions. The main function provides inputs for the sub-functions, executes the NP solver, and plots the results. One of the sub-functions calculates the Jacobian which is used in the

47

NR solver and the second calculates the forces on each node. The Jacobian matrix of first partial derivatives with respect to each variable is approximated using a simple first-order, finite-difference method. The force balance sub-function calculates the forces on each node using information about the size, properties and geometry of the network. All functions can be found in APPENDIX B with annotation.

Of the networks analyzed (i.e. single hexagon, seven, nineteen, and thirty-seven hexagon networks), we predicted the solution of stretched length by using the formula for the approximate analytical (non-dimensional) solution which is:

$$L = \frac{K_i - 2\gamma}{K_i - \dfrac{P}{\dfrac{\sqrt{3}}{2}\left(\dfrac{3}{2}C_F - 1\right)}}.$$

C_F represents the number of springs cut when cutting the pressurized network horizontally through the center as in Figure 20. This equation will be used to predict the approximate analytical solution for the networks studied in Section 4.4 This equation has two regimes that depend on the value of γ for very large networks or as C_F goes to infinity:

If $\gamma < \frac{K_i}{2}$ Then for L>0, Pcrit <P <Pmax.

If $\gamma > \frac{K_i}{2}$ Then for L>0, P > Pmax.

K_i is a "typical" value of a spring constants, for our case we set $K_i = \frac{1000N}{m^2}$. Pcrit is the minimum inflation pressure required to cause the network to become patent and Pmax is the maximum inflation pressure that causes stretched length L to

48

approach positive infinity. The first case seems more physiologically relevant due to the pressure bounds. On the other hand, the second case may be more relevant due to the surface tension and spring constant relationship. It is as yet unclear, which regime would be more physiologically applicable and under what specific conditions.

Section 4.2. Single hexagon network

To validate the code, we first derived equations for and modeled a "dry" single hexagon (i.e. in which the effects of surface tension were not included). To start, we input an initial guess of an equilibrium hexagonal shape and incrementally increased the pressure (see Figure 22). Note, that we "pinned" the top right hand node (node 1) to fix the hexagon's position in space. The corresponding nodes were numbered from one to six counting clockwise around the hexagon. The table below compares the dimensional values of computational and analytical solutions.

Pressure (N/m^2)	L (m): computational	L(m): exact analytical solution	Error %
0.1	1.764	1.764	7.16E-12
0.08	1.530	1.530	-1.6E-12
0.05	1.276	1.276	-8.2E-13
0.03	1.149	1.149	-3.7E-13
0.02	1.095	1.095	-3.7E-13

Table 8: Exact analytical solutions for the single hexagon, with single hex k=0.2N/m, γ=0 N/m and L0=1(m). Error was calculated as $\frac{computational-exact}{exact} * 100$.

In Figure 22, the coordinate axes are omitted for clarity. This plot confirms that the network size increases with increasing pressure, as expected. We also

49

verified that this indeed was an equilibrium solution confirming that all edge

lengths were the same and that the sum of forces on each node was zero.
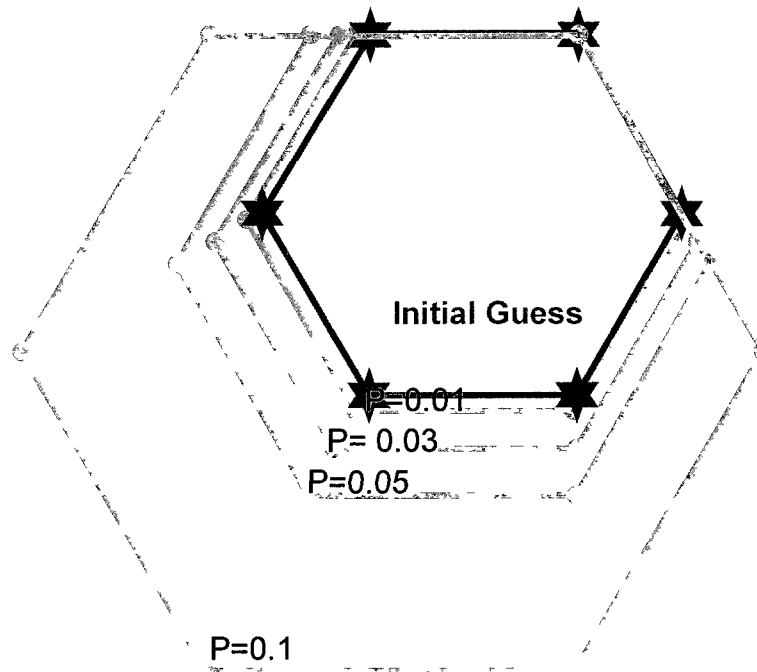
Figure 22: Incremental progression in network size with increasing pressure. The red hexagon (with stared points) is the initial guess and the green hexagons (with round points) are solutions for each pressure. k=0.2N/m, γ=0N/m and L0=1(m) and pressure has units of N/m².

As another test, we altered the initial guess and iteration number. The aim of

altering the initial guess was to test the robustness of the code to find the

equilibrium shape with an inflating pressure. As shown in Figure 23, even with a

differently shaped initial guess, the computational model converges to a

hexagonal shape. However, note that the hexagons rotate about the pinned

node. This indicates that although the code is able to find an equilibrium solution,

there are many equilibrium solutions that satisfy the force balance. Therefore,

depending on the final iteration count, different orientations are displayed. We

confirmed that all the edge lengths were the same, and that the net force on each

node was zero to verify that the solution was the equilibrium solution.
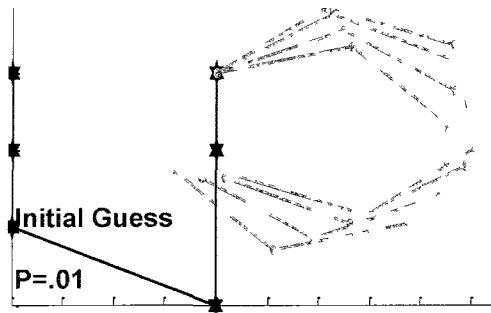
Figure 23: Rectangular initial guess for hexagon with pressure. Each hexagon is the solution for P=0.01 N/m², k=0.2 N/m, γ=0 N/m and L0=1 m and with different final iteration count.

In addition, we also investigated how the network would deform in the presence

of material heterogeneities. Keeping the inflating pressure constant, we altered

the spring constant of the bottommost spring to be less than the neighboring

springs, and found that increasing a spring constant in one element caused that

element to resist expansion. Decreasing a spring constant caused the element to

be more compliant, compared to the adjacent springs as shown in Figure 24.
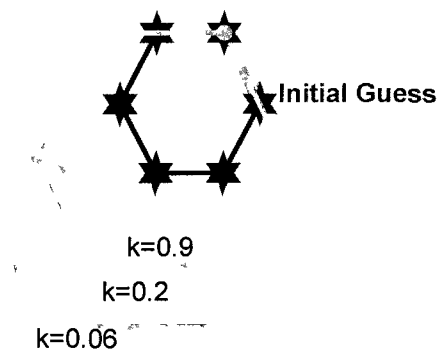
Figure 24: Single hexagon with equal inflation pressures and different spring constants for the bottommost spring (all other springs were k=0.2 N/m) γ=0 N/m, L0=1 m for P=0.01(N/m²) for all cases.

As a final note, we also documented the convergence of the solution of the single hexagon, for dimensional non-physiological values of P=0.03N/m^2, K=0.2N/m, and L0=1m for various iteration number.

Iteration	L0 (m)	K (N/m)	P (N/m^2)	L (m) Analytical	L (m) Computational	Error %
1	1	0.2	0.03	1.1493	1.1510	0.14463
5	1	0.2	0.03	1.1493	1.1493	1E-04
10	1	0.2	0.03	1.1493	1.1493	7.9E-06
100	1	0.2	0.03	1.1493	1.1493	-3.7E-13
200	1	0.2	0.03	1.1493	1.1493	-3.7E-13

Table 9: Relative error for the single hexagon with different iteration number. There was not surface tension for this test. Error was calculated as $\frac{computational-exact}{exact} * 100$.

The relative error clearly decreases for increasing iteration count. Depending on the exactness of desired outputs, iteration count between 10 and 100 are sufficiently converged to the exact solution.

Section 4.3. Seven hexagon network

After validating our model of a single hexagon, we then examined a seven hexagon network. For this network we incorporated pressure, surface tension, and changes in the spring constants and used physiological estimations for parameters. Network area was calculated with a built-in Matlab function called *polyarea*, which calculates the interior area of the polygon defined by the pleural node x and y coordinate positions. With the solution derived from the force balance we can calculate the exact dimensional solution for the seven hexagon network and compare that value to the computational solution (see Table 10).

Pressure (N/m^2)	L (m) computational	L (m) exact analytical solution	Error %
400	6.391E-05	6.326E-05	-1.02
450	6.943E-05	6.864E-05	-1.15
500	7.601E-05	7.501E-05	-1.31
550	8.396E-05	8.269E-05	-1.52
600	9.377E-05	9.210E-05	-1.78

Table 10: Comparison an analytical and computational solutions of stretched length for the seven hexagon network. γ is 0.03N/m for all cases and K=1000N/m. Error was calculated as $\frac{computational-exact}{exact} * 100$.

4.3.1 Variations in spring constants

First, we will look at the effect of changing the spring constants for the *entire* network. In Figure 25, we see a pressure versus area (PA) plot and three corresponding images of the seven hexagon network. The circle dotted curve and largest network correspond to the lowest spring constant of the three; the smallest network and long dashed curve correspond to the network with the highest spring constant. It can be seen that in networks with the same inflation pressure but different spring constants, stiffer networks require more pressure to inflate than the less stiff networks, as expected. The axes are non-dimensionalized and scaled to start area and pressure at unity. Pcrit is the lowest pressure (500N/m^2) and Acrit is the smallest circumferential area at Pcrit.
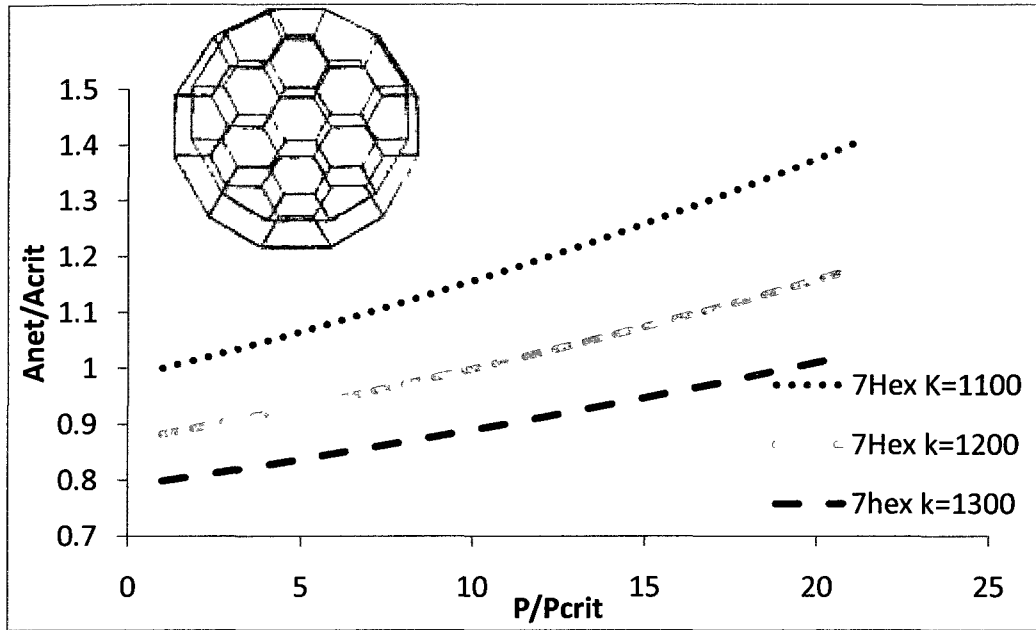
Figure 25: This figure shows PA curves for three different "dry" network-wide spring constants. The circle dotted curve shows the spring constant of the interior springs (K_i) to be 1100N/m, the medium dashed curve, K_i=1200 N/m, and the long dashed curve, K_i=1300 N/m. Corresponding network result also shown in corresponding colors.

Notice that a seemingly very small change in spring constant magnitude results in larger changes as pressure increases. For the seven hexagon network as well, we studied convergence for one case. We used physiologival, dimensional values of L0 = 50 microns, K =1000 N/m, and P=500 N/m^2 and set the surface tension magnitude to be zero. We also considered the average interior L to be the computational solution of stretched length.

Iteration	L (m) Analytical	L (m)Computational	Error%
1	7.601E-05	7.280E-05	-4.22032
5	7.601E-05	7.501E-05	-1.30933
10	7.601E-05	7.501E-05	-1.31229
100	7.601E-05	7.501E-05	-1.31258
200	7.601E-05	7.501E-05	-1.31258

Table 11: Relative error for the seven hexagon network with different iteration number. There was not surface tension for this test. Error was calculated as $\frac{computational-exact}{exact} * 100$.

It is clear that the computational solution converges to the analytical solution with increasing iteration number. For our analysis, we chose iterations between 10 and 100 to be well converged, and sufficiently close to the analytical solution. This one percent error is most likely due to round off error resulting from the very small dimensions of the unstretched lengths and the very large magnitudes of pressure and surface tension interacting.

4.3.2 Variations in surface tension

Networks with non-zero surface tension are of primary interest. In Figure 26, we again can see that with increased surface tension, the network becomes stiffer. We have assumed surface tension force to act parallel to the resistive spring force but this does not mean that increasing surface tension acts as if the spring constant was made stiffer. Rather, the spring force depends on ΔL and the force due to surface tension is independent of ΔL even though it is parallel to the spring force. The equivalent network picture would be similar to that in Figure 25.
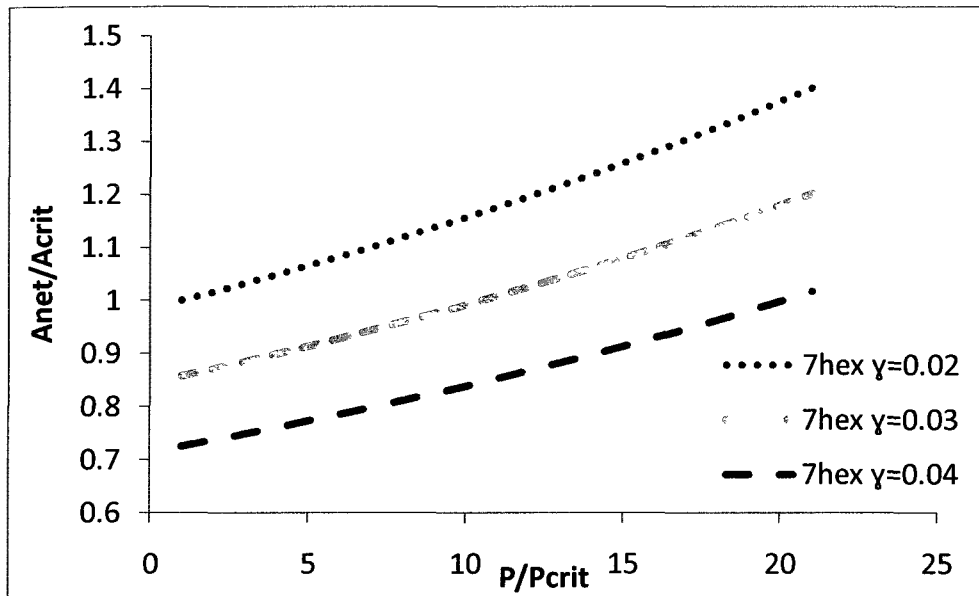
Figure 26: This plot shows the PA curves for three different network-wide γ values. The circle dotted curve shows $\gamma = 0.02\text{N/m}$, the medium dashed curve shows $\gamma = 0.03\text{N/m}$, and the long dashed curve shows $\gamma = 0.04\text{N/m}$. For these network simulations, $K_i = 1100\text{N/m}$.

Here also, the general trend in wet networks is seen as a lessening of slope, meaning more pressure is required to inflate a "wetter" network to a given area.

4.3.3 Variations in both spring constants and surface tension

For completeness, we also compared networks having various spring constants and various surface tensions. Plotted in Figure 27, are curves of a network with two different spring constants, both with different surface tension magnitudes.
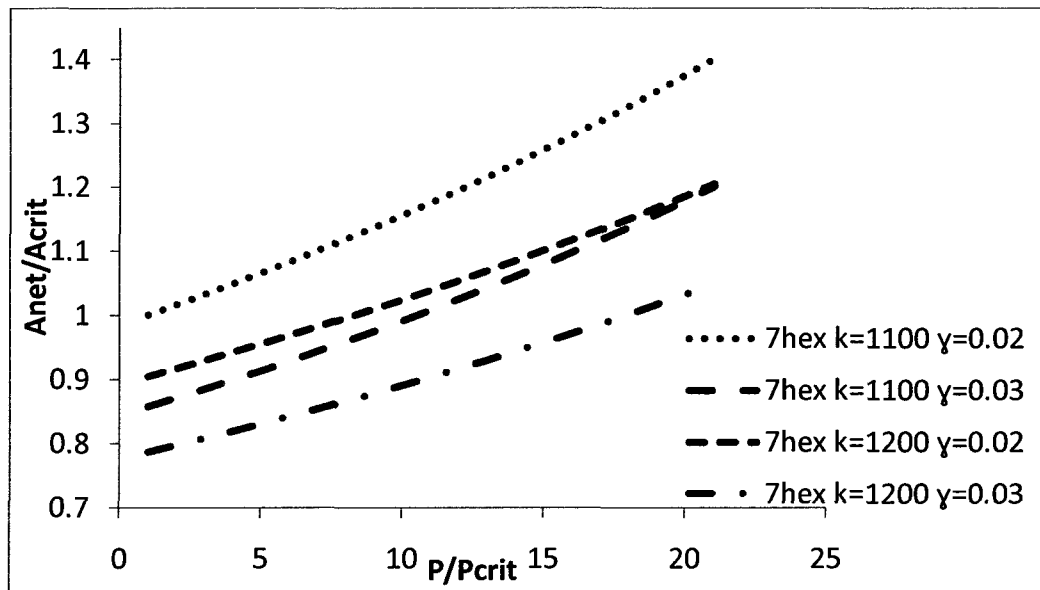
Figure 27: Various γ and K PA plots. The pairs of curves with parallel slopes have the same K, the top two are K=1100N/m and the bottom two, K=1200 N/m. There are also two cases for γ, γ=0.02 and γ = 0.03.

The curves with parallel slopes have the same spring constant, but are shifted down as γ increases. Comparing the two cases of spring constants, the curves with the greater spring constant have a slightly less steep slope. These trends indicate that changing surface tension greatly changes the area of the network, but increasing the spring constant magnitude causes the slope to be shallower. Intuitively, surface tension makes the networks more difficult to inflate, and the changing the spring constants essentially changes the elastic modulus of the network.

Section 4.4. Larger networks

Notice also the increasing slope in the plots as pressure increases. In the low pressure region, increasing pressure one unit results in a small area increase. In the higher pressure region, increasing the pressure one unit results in a much

greater increase in network area. To clarify, these networks composed of time independent, linearly elastic springs (wet or dry) become "easier" to inflate with increasing area. Liken this to a balloon that is difficult to inflate when first starting to inflate, then gets easier to blow up as the volume increases. With different spring properties (e.g. nonlinearly elastic or viscoelastic) this property could be changed, we could instead easily configure a network to decrease in compliance with inflation pressure.

The following plots show PA curves for various sized networks with various spring constants and surface tensions, a plot of critical pressure required to inflate the networks, a maximum pressure before the linearity of the springs causes the stretched length to go to positive infinity, and a table comparing *approximate* analytical and computational solutions. The values for stretched length L were obtained from the (non-dimensional) approximate analytical solution equation:

$$L = \frac{K_i - 2\gamma}{K_i - \frac{P}{\frac{\sqrt{3}}{2} \frac{C_F}{\left(\frac{3}{2}C_F - 1\right)}}}.$$

As can be seen in the table below, the approximate analytical and computational solutions are not expected to match for smaller networks, but it seems that with increasing network size solutions may become more similar.

58

Network size	L^*_0	K^*	C_F	γ^*	P^*	L^*	Computa-tional L^*	Error%
1	1	0.2	2	0	0.03	1.21	1.2	0.78
7	5.00E-05	1000	4	0.03	500	1.17E-04	1.03E-04	387.44
19	1.50E-04	1000	6	0.03	500	6.01E-04	1.89E-04	51.76
37	5.00E-05	1000	8	0.01	500	2.29E-04	7.85E-05	46.06

Table 12: Approximate solutions for different networks. Computational solutions for small networks are not expected to match approx. analytical solution. But as network size increases, approx. analytical solution is hypothesized to approach computational solution. L's have units of m, K N/m, γ N/m, P N/m^2, and network size is m^2.

For the nineteen and thirty seven hexagon networks, we found the forces on each node for these specific cases was slightly less than 10^{-3}, (compared to the spring constant term on the order of 0.028 and 0.012, respectively,) and considered solutions on this order to be "zero" solutions. Also the sum squared error of the nodal forces was slightly less than 10^{-6} for both cases. So although the approximate analytical and computational solutions do not match, the computational model provided solutions that converged to satisfy the zero nodal force balance.

To identify any trends, we plotted three sized networks (seven, nineteen, and thirty seven hexagons) for various spring constants and surface tensions. The vertical axis is a normalized area scaled to unity. Each network area was scaled by the corresponding critical area (Acrit). For example, the thrity seven hexagon network data was scaled by the area of the thrity seven hexagon network at the smallest γ or K. So each network area was normalized to unity. Pressure was also normalized to unity in the same way for Figure 28 and Figure 29.

59
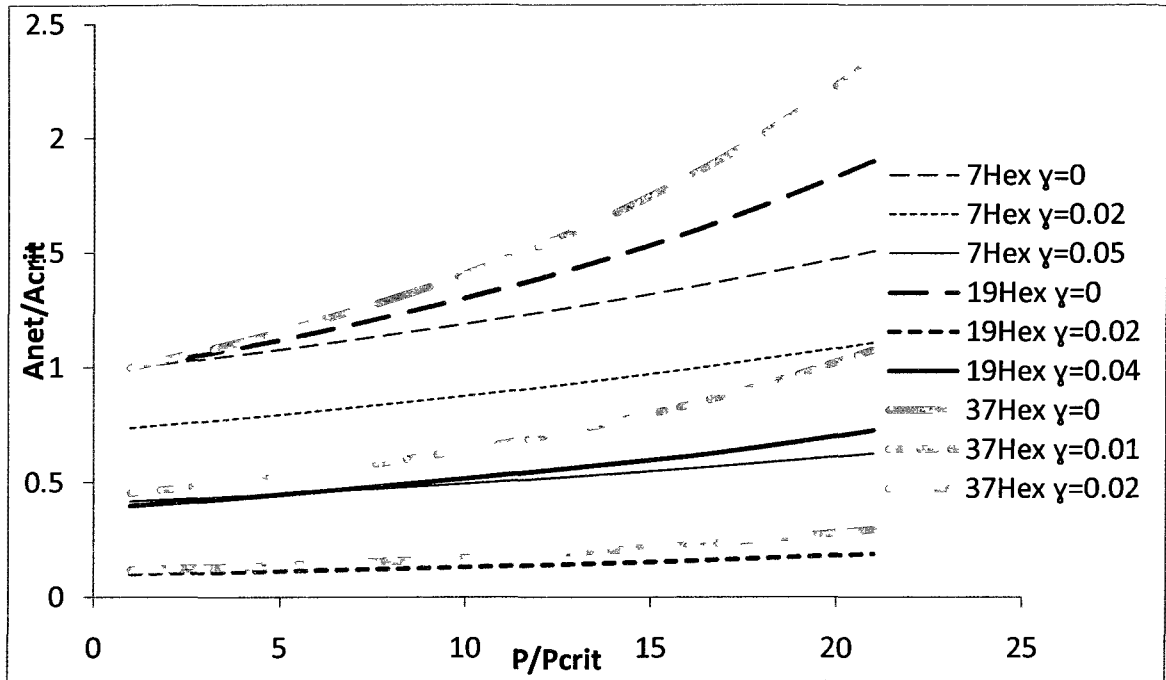
Figure 28: Various γ in three different sized networks. Various surface tension magnitudes for three differently-sized networks for K=1000N/m. The short line in the legend represents the long dashed curve, the long line represents the solid, continuous line with non-dimensionalized axes.

For each of the three networks, the cases with the lowest surface tension have the greatest area, and the cases with the highest surface tension have smaller areas. Figure 29 shows the relationships between the three networks and various spring constants.
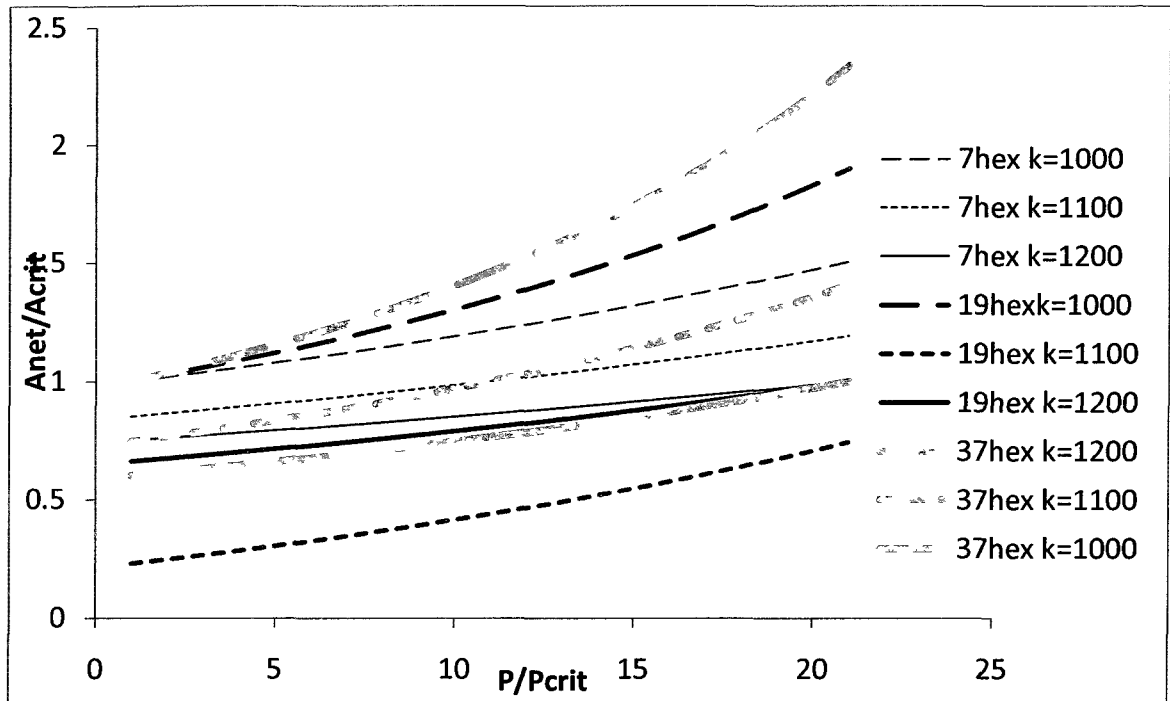
Figure 29: Three different networks with various spring constants. Various spring constant magnitudes for three differently-sized networks for γ=0. The short line in the legend represents the long dashed curve, the long line represents the solid, continuous line with non-dimensionalized axes.

The cases with the smallest spring constant shoe the greatest area, and increasing spring constants results in less area for a given pressure, as expected. Note the nineteen hexagon network for K=1100 as the only outlier.

We also plot the minimum pressure required for initial inflation of the networks and a maximum pressure where the stretched length solution approaches positive infinity as another way to understand the network wide properties. If the force due to surface tension increases in any size network, the initial pressure required to inflate the network would also logically increase. Figure 30 shows that as the surface tension force increases in the networks, so too does the pressure required to inflate the networks. The seven hexagon network most clearly shows

61

this trend, and although the thirty seven hexagon network does not show as dramatic an increase γ does increase from $\frac{0N}{m}$ to $\frac{0.02N}{m}$ while the pressure increased from $\frac{74N}{m^2}$ to $\frac{83N}{m^2}$. However this plot shows a surface tension effect opposite to what we would expect. We hypothesized that because larger networks have more membranes and hence, more fluid lining the membranes, that as network size increased so would the over-all pressure required to initially inflate the network. But what we see below is that a larger network requires *less* pressure to inflate. We assume this is effect is caused by the dominance that the pleural edges have on the smaller networks. The larger networks are less dominated by what happens at the pleural surface, and although the net surface tension force may be greater in the larger network, its dynamics are dominated by the internal membranes as opposed to the pleural membranes.
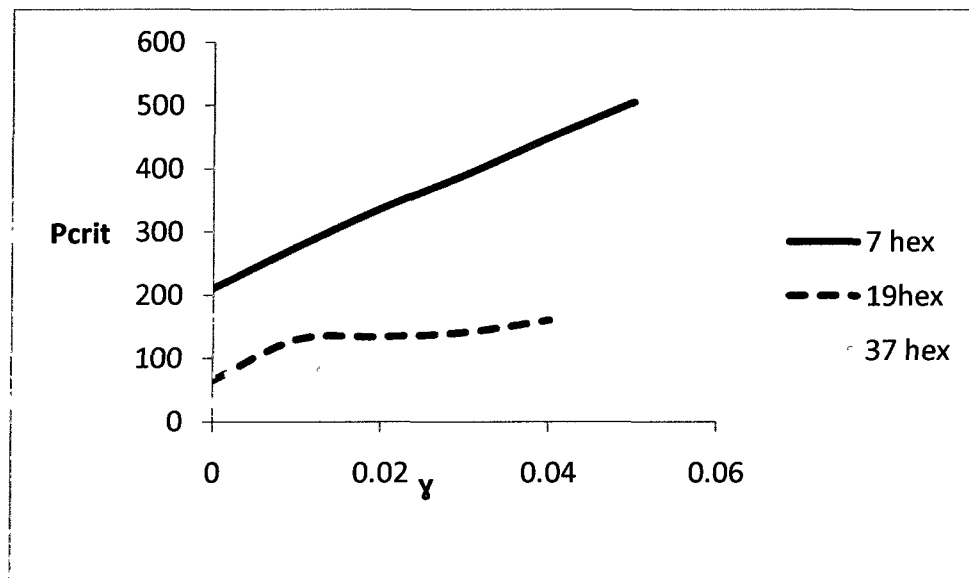
Figure 30: Critical pressure versus force due to surface tension.

We also examined the relationship between the maximum inflation pressure and

surface tension. For all cases the spring constant was $\frac{1000N}{m}$. The smaller the

network, the greater the surface tension can be with a convergent solution. For

the thirty seven hexagon network, the solution only converges for $\gamma < 0.02$,

hence the curves terminate at the maximum γ for which the networks converge.
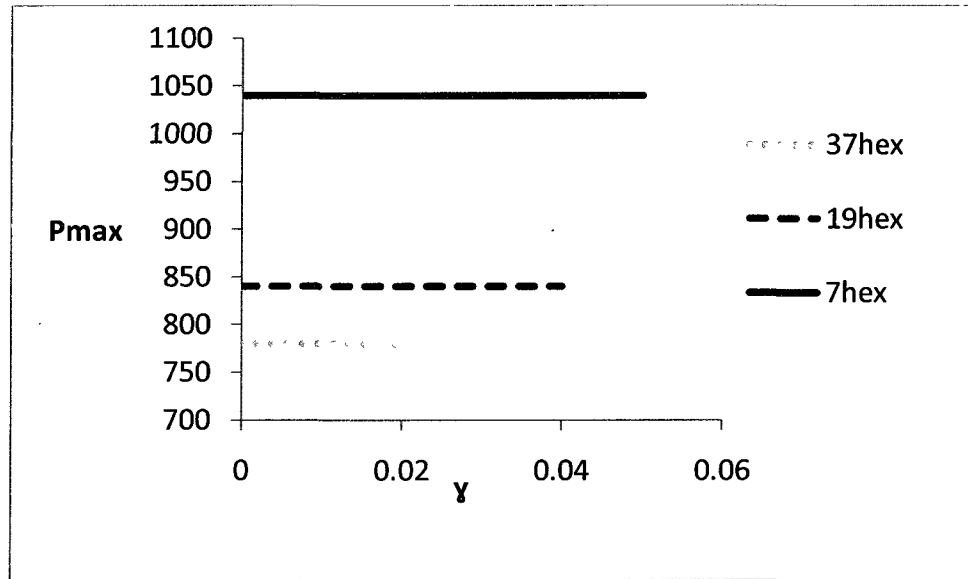
Figure 31: Maximum pressure that a network can sustain before solution of stretched length shoots to positive infinity.

In order to make appropriate first guesses for each new pressure, the analytical

solution is used as the initial guess. As an example the non-dimensional exact

analytical solution for the seven hexagon is:

$$L = \frac{(2K_S - \sqrt{3}K_B)}{2\sqrt{3}(K_S - K_B) - P}$$

Equation 36

The figures above show the scaled/ non-dimensionalized circumferential area

versus pressure. If we look at Equation 36, we can see that the numerator will be

63

positive for $K_B < K_s$, which in fact is the case. Because these spring constants do not change with pressure, the numerator is constant for all pressure. But we also see that as the pressure increases the denominator approaches positive infinity. L approaching infinity does not correspond to a logical physical situation and therefore we exclude plots past this maximum.

Just as very large pressures cause the stretched length to approach positive infinity, increasing the magnitude of the surface tension causes the solution to become negative. Recall the non-dimensional equation

$$L = \frac{\left(2K_s - \sqrt{3}K_B\right) - \gamma\left(2 - \sqrt{3}\right)}{2\sqrt{3}(K_s - K_B) - P},$$

we see that if $\gamma > 2K_s - \sqrt{3}K_B$ stretched length will be negative. Negative L does not correspond to a physical solution; since we have chosen only to consider expanded networks and disregard any negative solutions.

The exact analytical and computational solutions match to (round off error) for the single and seven hexagon solutions. The primary solution discrepancies are between the approximate analytical and computational solutions for nineteen and thirty seven hexagon networks, and lack of consistent trends in the nineteen hexagon network. The approximate analytical solutions, although not precisely equal to the computational solution, are useful to provide close initial guesses for computing solutions for larger networks because of the comparable order and we hypothesize will approach the computational solutions as the network size increases. In addition, the lack of trends of the nineteen hexagon network in the

various surface tension and spring constant plots may be due to a slightly

different unstretched length as compared to the other networks.

CHAPTER 5.

Future Work

Section 5.1. Dynamics

As introduced in 2.4.2, we are ultimately concerned with understanding the mechanics of a dynamic lung. While static force balance analysis has provided us with a solid foundation for a lung model, the next logical step will be to include time dependence, which will allow us to incorporate viscoelastic material properties and other viscous effects from the thin film lining the lung.

Additionally, we modeled a single tri-junction (where three hexagons meet) dynamically. Each element was modeled as a linearly elastic spring that could experience a time-dependent damping following the damped harmonic oscillator equation:

$$0 = M\ddot{x} + C\dot{x} + Kx$$

We were able to fix the outside edges and perturb the center node to initiate oscillations, see Figure 32. By converting this second order differential equation to a first order differential equation then using a built in Matlab ODE solver, we were able to capture the dynamics of this coupled system.
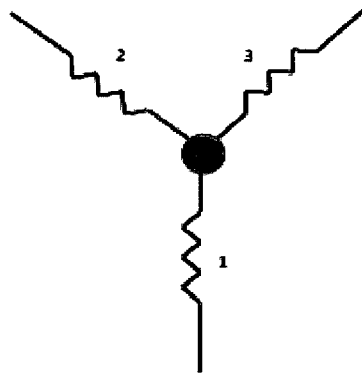
Figure 32: Three coupled, damped harmonic oscillators modeling a septal tri-junction.

Physiologically, a septal tri-junction would not move from the center, instead the

dynamics would come from inflating and deflating an entire network.

Nevertheless, we modeled this system and generated phase plots like in Figure

33.
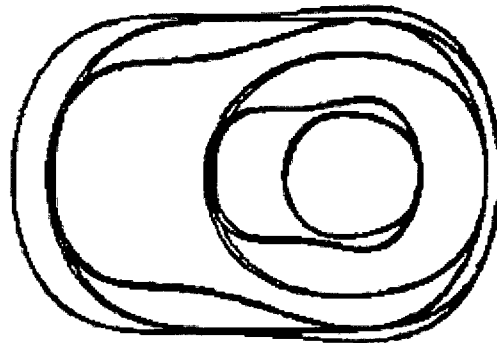
Figure 33: Phase plot of X position and velocity for coupled oscillators. Note the concentric cycles indicating some energy conservation.

For a simple pendulum with no friction, the phase plot can look oblate or even

circular which indicates some sort of energy conservation. In the figure above, it

seems there is energy conservation occurring, but in an irregular way. It would be

exceedingly interesting to dynamically model coupled oscillators that more

67

closely approximate cycling in the lung, and would surely be part of this project's future.

Section 5.1. Experiment

A natural complement to a computational model would be an experimental model of a small network of alveoli. Potential experiments may be: a method to study the fluid lining in the corners of alveoli, a sealed and pressurized single hexagon, a micro-etched, to-scale network of channels, even a rudimentary linked, rubber band model.

Section 5.2. Material properties

In addition to viscous effects of the fluid lining, properties of the lung tissue itself can be modeled as nonlinearly elastic or viscoelastic (Fung & Sobin 1972; Gardel et al. 2004; Hoppin et al. 1998). Recall samples of PV curves. The hysteresis in these curves is due to the viscoelasticity of lung tissue and liquid lining. Specifically there is a time-volume dependence that causes the lower part of the curve (inhale) to be different than the top half of the curve (exhale). A nonlinear elastic model may not be able to capture this "material memory" of the PV curve's marked hysteresis, but a time dependent viscoelastic model would show definite hysteresis.

Section 5.3. Local deformation

In the future, we would seek to determine more specific effective properties of our network composed of isotropic or heterogeneous materials. The networks studied in this way would be similar to that of Suki and Bates 2008.
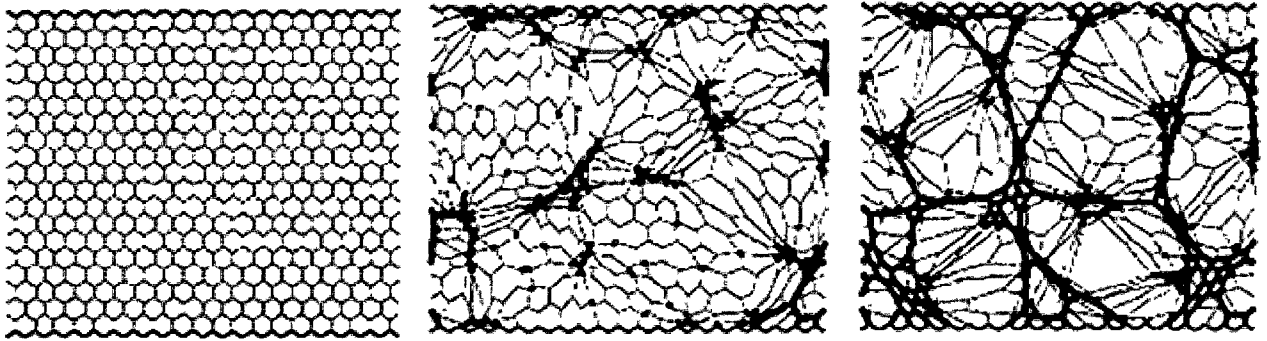
Figure 34: These three images show a progression of spring stiffness from uniform spring constants on the left to highly varied spring constants on the right (from Suki & Bates 2008).

We would predict that curves of progressively heterogeneous networks would change slopes on both the inhale and exhale. Networks with stiffer spring constants would locally deform the network and cause the PV or compliance curve to have a less steep slope, meaning more pressure would be required to inflate to a lesser volume, modeling pulmonary fibrosis. The inverse would be true for a network with randomly distributed compliant springs or membranes, modeling emphysema. As a first look we cut one spring in the nineteen hexagon network. It is conceivable that this network would have different effective properties than that of a heterogeneous network without any cut springs.
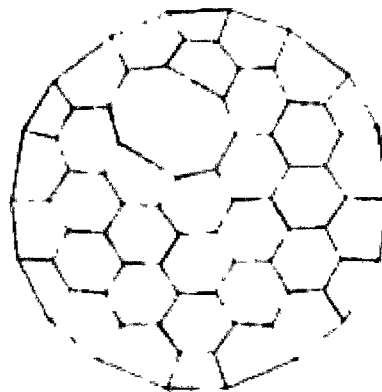
Figure 35: Nineteen hexagon network with one cut spring.

In addition to network heterogeneity, the pressure distribution could also be locally changed. If a network was composed of isotropic membranes but had a pressure distribution that was not equal in all unit cells, then the network would also tend to resemble a heterogeneous network. This change would alter the stress distribution in the network and may change the PV and compliance curves as well.

Section 5.4. Geometry

To more closely approximate the lung, our model could also have variable geometry. The model could have more hexagons, shapes other than hexagons, could be three dimensional and could account for the presence of other lung structures like peripheral airways and alveolar ducts.

Section 5.5. Numerical solver

At this stage in the development of the model, we have found one of the simplest and most straightforward numerical solvers to be effective. Because the Newton-Raphson method is locally convergent, it can quickly diverge if the initial input guess to the solver is too far from the final solution. However, for our model, we found it converges very quickly to a solution. As potentially useful for larger and more complex models, we coded a globally convergent variation on Newton-Raphson that included line searching and backtracking. *Numerical Recipes 3rd Ed.* served as the primary reference for this script (Press et al. 2007). This code can also be found in APPENDIX B. Moreover, we would optimize and automate

how the adjacency matrix, XY points, node numbering and initial guess based on

the analytical solution is generated.

CHAPTER 6.

Conclusion

Section 6.1. Discussion of dry and wet networks

We have found that mechanics of networks composed of linearly elastic springs and a constant surface tension force is somewhat predictable, once intuition is established. The effective properties would not be as predictable with different spring and surface tension properties. *In vivo*, surface tension does vary. It can vary because of the concentration of surfactant or volume of fluid. At one extreme, a fluid filled lung has no surface tension and at the other extreme a lung with no surfactant has very high surface tension. In a healthy lung however, Type II epithelial cells release surfactant, initiated by calcium ion activated pathways and mechano-transduction[2], causing surface tension to vary only slightly (Rice 2000; Ashino et al. 2000). In addition, extractions of surfactant, measured in a Wilhelmy plate set-up, will display an *area* dependence.

---

[2] Essentially, a deep breath signals Type II cells to release surfactant, which decreases alveolar surface tension, making the next breath easier!
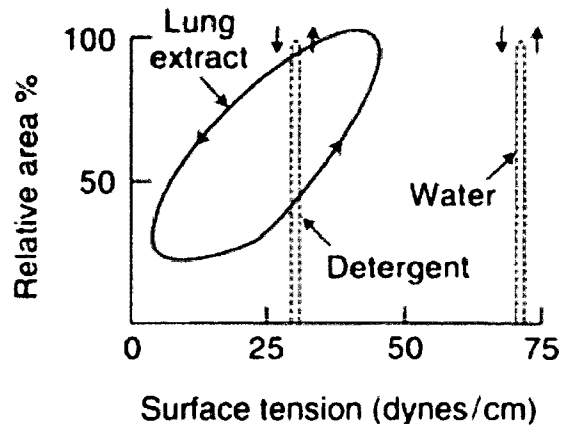
Figure 36: Shows area dependence of lung washings from (West 2005).

In fact the plot is hysteretic. In a complete lung model, this characteristic must be taken into account when studying alveolar mechanics: γ would be a function of area not constant.

Section 6.2. Intuitive findings and model discussion

In summary, we found different types of solutions useful for different aspects of this study. The exact analytical solutions were useful for verifying and validating the computational mathematics for the single and seven hexagon networks. The approximate analytical solutions were also useful in validating the computations, but we intended the approximate analytical solutions to be close approximations of the computational solution in order to predict trends and PV curves of much larger networks analytically. Although the approximate analytical solutions are not comparable to the computational solutions they may prove to be very useful as initial guesses to more complex computations. And of course, now that our computational mathematics have been validated, we can move to any size network or any other progressions as mentioned in the Future Work chapter.

73

Furthermore, the plots in Section 4.4 show generally, intuitive trends. However the nineteen hexagon network seems to have non-intuitive properties in the various spring constants and surface tension plots, but it does fall into place in the critical and maximum pressure plots. Recall the discussion of two regimes for the analytical and computational solutions and the solution for the "wet" seven hexagon network:

$$L^* = \frac{\left(2K_S^* - \sqrt{3}K_B^*\right)L_0^* - \gamma^*(2 - \sqrt{3})}{2\sqrt{3}(K_S^* - K_B^*) - P^*}.$$

From this equation we can see that the numerator must satisfy

$$\gamma^* > \frac{\left(2K_S^* - \sqrt{3}K_B^*\right)L_0^*}{2 - \sqrt{3}}$$

We will call this critical value of γ^*, γ_{crit}^*. All results reported in this paper have been for $\gamma^* < \gamma_{crit}^*$. The plot below shows curves for the two regimes. Essentially we see that if the magnitude of surface tension gets large enough thtne the network as a whole is dominated by surface tension and the magnitude of the spring constants do not have a large impact. Note, the lengths in the plot below are lengths of a single alveolar septa.
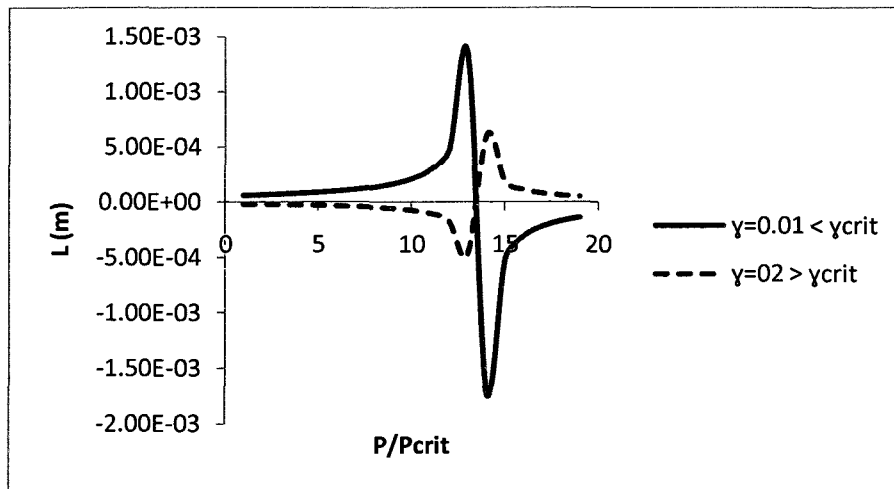
Figure 37: Two surface tension regimes.

Two additional observations are relevant. First, we confidently predict that analytical solutions for larger networks could be found if rounder external geometries were used as opposed to the "straight edge" geometry. And because the network would be rounder, a high degree of symmetry would also be expected to facilitate an exact analytical solution. Secondly, physiological/dimensional (and non-physiological) values can be used in the computations. The value of using physiologically derived values is that PA or PV curves can be directly compared to those obtained from patients *in vitro,* a highly valuable comparison when studied by clinicians or treatment of disease is involved.

In conclusion, we have shown how a linearly elastic spring model with surface tension and pressure effects is an appropriate first step in modeling alveolar mechanics. Although in its current state, this model is quite limited and only vaguely resembles a section of lung, the parameters and inputs can be changed

straightforwardly. This model forms the foundation to a more complex and even

dynamic computational model of alveolar micromechanics.

APPENDIX A

For a clearly presented and easily understandable lesson on how lung pressure and volume are measured in the living human lung, see the references: Johns Hopkins' School of Medicine Interactive Respiratory Physiology: Alveolar Pressure (Johns Hopkin's School of Medicine 1995) and Airway structure and function by SpirXpert (SpirXpert: Philip H. Quanjer 1999), and Textbook of Medical Physiology by Guyton and Hall (Guyton & Hall 1996).

The left plot in Figure 38 shows that rough Pressure-Volume curves can be generated from plots of data like the right plot in Figure 38.
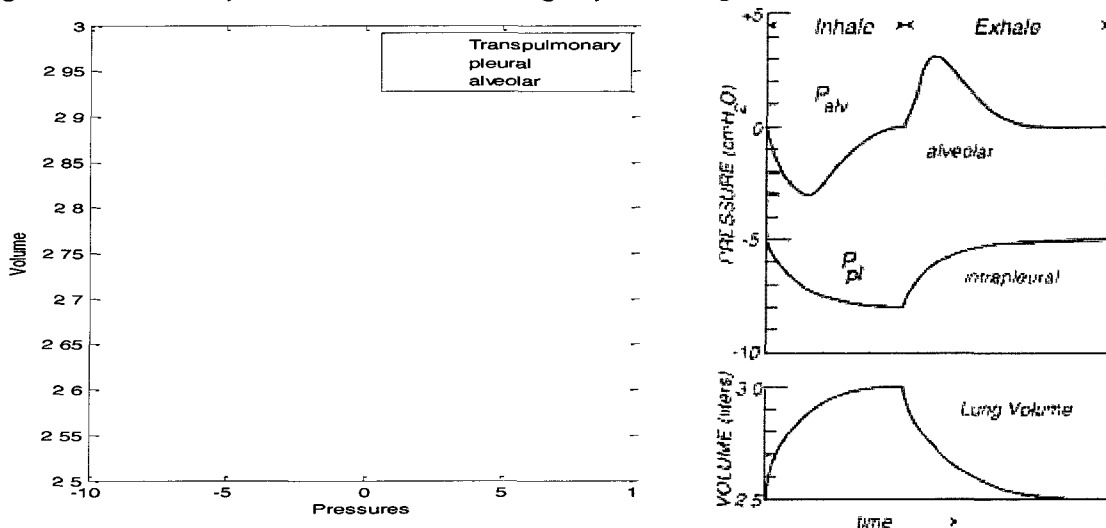
Figure 38: PV curves plotted from the data in the right graph. These are two different ways of plotting the same data.

Left plot in Figure 38 was generated from the following Matlab code:

```
INPUT
volume=[2.85 2.95 2.98 3 2.73 2.61 2.53 2.52 2.51 2.5];
pleural_pressure=[-5 -7 -7.7 -7.9 -8 -6 -5.5 -5.3 -5.2 -5.1 -5];
alv_pressure=[0 -3 -2 -.5 0 3 1.7 .5 .2 0 .1];
transpulmonary_pressure=alv_pressure-pleural_pressure;

OUTPUT
plot(transpulmonary_pressure, volume); hold on
plot(pleural_pressure, volume, 'r'); hold on
plot(alv_pressure, volume, 'g'); hold on
xlabel('Pressures')
ylabel('Volume')
legend('Transpulmonary', 'pleural', 'alveolar')
```

APPENDIX B

In this appendix there are four Matlab functions. The first one, "Please_Work" is the main function, uses Newton-Raphson solver and plots solution by calling the other two functions. The second function, "Force_eq" calculates the nodal force balance and "Jac" calculates a finite difference Jacobian. The fourth function "newt_temp" is a globally convergent version of Newton Raphson.

"Please_Work" is the calling function.

```
function [inner_edge_calculated plsmall_edge_calculated plbig_edge_calculated]...
    =wet_SL_please_work_seven_hex( p, ki, anafactor, sor, maxiter)

%Initial Guess
xy=anafactor.*[4,6.49519052800000;4.75000000000000,6.06217782600000;5.25000000000000,
5.19615242300000;5.25000000000000,4.33012701900000;4.75000000000000,3.464101615000
00;4,3.03108891300000;3,3.03108891300000;2.25000000000000,3.46410161500000;1.750000
00000000,4.33012701900000;1.75000000000000,5.19615242300000;2.25000000000000,6.062
17782600000;3,6.49519052800000;3.25000000000000,6.06217782600000;3.75000000000000,
6.06217782600000;4,5.62916512500000;4.50000000000000,5.62916512500000;4.7500000000
0000,5.19615242300000;4.50000000000000,4.76313972100000;4.75000000000000,4.3301270
1900000;4.50000000000000,3.89711431700000;4,3.89711431700000;3.75000000000000,3.464
10161500000;3.25000000000000,3.46410161500000;3,3.89711431700000;2.50000000000000,
3.89711431700000;2.25000000000000,4.33012701900000;2.50000000000000,4.763139721000
00;2.25000000000000,5.19615242300000;2.50000000000000,5.62916512500000;3,5.62916512
500000;3.25000000000000,5.19615242300000;3.75000000000000,5.19615242300000;4,4.7631
3972100000;3.75000000000000,4.33012701900000;3.25000000000000,4.33012701900000;3,4.
76313972100000;];

xy=reshape(xy,72,1);
xytemp=[xy(2:36); xy(38:end)]';
NN=length(xy);
xyoldtemp=xytemp;

for n=1:maxiter
    xynewtemp= xyoldtemp -sor.*(wet_SL_jac_seven_hex( p, ki, anafactor,xyoldtemp)...
        \wet_SL_force_eq_seven_hex(p,ki,anafactor, xyoldtemp))';
    xyoldtemp = xynewtemp;
    new_force(n)=sqrt(sum((wet_SL_force_eq_seven_hex(p,ki,anafactor, xynewtemp)).^2));
end

forces_in_network=wet_SL_force_eq_seven_hex(p,ki,anafactor, xynewtemp);

close all
set(0,'DefaultFigureWindowStyle','docked')

xynew=NaN(1,72);
xynew(1)=xy(1);
xynew(2:36)=xynewtemp(1:35);
```

```matlab
xynew(37)=xy(37);
xynew(38:end)=xynewtemp(36:end);

figure(1)
stem(forces_in_network);
title('Plot of forces=feval(f,xynewtemp)','FontSize',12,'FontWeight','bold');
xlabel('Node Number (remember to +1)','FontSize',12,'FontWeight','bold');
ylabel('Force','FontSize',12,'FontWeight','bold');

figure(2)
plot(new_force);
title('Sum Error=sqrt(sum((force eq seven hex(xynewtemp)) ^2))','FontSize',12,
        'FontWeight','bold');
ylabel('Force','FontSize',12,'FontWeight','bold');

figure(3)
adjacency = zeros(N,N);
connections_sparse=sparse([1  1  1   2  2  2  3  3  3  4  4  4  5  5  5  6  6  6  7  7  7  8
8  8  9  9  9  10 10 10 11 11 11 12 12 12 13 13 13 14 14 14 15 15 15 16 16 16 17
17 17 18 18 18 19 19 19 20 20 20 21 21 21 22 22 22 23 23 23 24 24 24 25 25 25
26 26 26 27 27 27 28 28 28 29 29 29 30 30 30 31 31 31 32 32 32 33 33 33 34 34
34 35 35 35 36 36 36],
            [12 2  14  1  3  16 2  4  17 3  5  19 4  6  20 5  7  22 6  8  23 7  9  25
8  10 26 9  11 28 10 12 29 11 1  13 30 14 12 13 15 1  14 16 32 15 17 2  16 18 3
17 19 33 18 20 4  19 21 5  20 22 34 21 23 6  22 24 7  23 25 35 24 26 8  25 27 9
26 28 36 27 29 10 28 30 11 29 13 31 36 32 30 31 33 15 32 34 18 33 35 21 34 36
24 35 31 27],108);

xy=reshape(xy,36,2);
gplot(connections_sparse,xy,' -r');
hold on

gplot(connections_sparse,xynew,' -g');
h=findobj('type','line');
axis square
set(h,'linewidth',2);
title('Resultant Shape due to Imposed Pressure ','FontSize',12,'FontWeight','bold')
legend('Initial Guess','Final Configuration','Location','SouthOutside')

inner_edge_calculated=((((xynew(32)-xynew(31)).^2+
        (xynew(32+NN/2)- xynew(31+NN/2)).^2)).^.5);
plbig_edge_calculated=((((xynew(7)-xynew(6)).^2+(xynew(7+NN/2)- xynew(6+NN/2)).^2)).^.5);
plsmall_edge_calculated=((((xynew(6)-xynew(5)).^2+(xynew(6+NN/2)- xynew(5+NN/2)).^2)).^.5);


end
```

"Force_Eq" calculates evey nodal force balance.

```
function [FXFYequations]=wet_SL_force_eq_seven_hex(p,ki,anafactor, xytemp)

%%%%Calculate L0 from P=0
xyeq=[4,6.49519052800000;4.75000000000000,6.06217782600000;5.25000000000000,5.19615
242300000;5.25000000000000,4.33012701900000;4.75000000000000,3.46410161500000;4,3.0
3108891300000;3,3.03108891300000;2.25000000000000,3.46410161500000;1.7500000000000
0,4.33012701900000;1.75000000000000,5.19615242300000;2.25000000000000,6.0621778260
0000;3,6.49519052800000;3.25000000000000,6.06217782600000;3.75000000000000,6.062177
82600000;4,5.62916512500000;4.50000000000000,5.62916512500000;4.75000000000000,5.19
615242300000;4.50000000000000,4.76313972100000;4.75000000000000,4.33012701900000;4
.50000000000000,3.89711431700000;4,3.89711431700000;3.75000000000000,3.46410161500
000;3.25000000000000,3.46410161500000;3,3.89711431700000;2.50000000000000,3.8971143
1700000;2.25000000000000,4.33012701900000;2.50000000000000,4.76313972100000;2.2500
0000000000,5.19615242300000;2.50000000000000,5.62916512500000;3,5.62916512500000;3.
25000000000000,5.19615242300000;3.75000000000000,5.19615242300000;4,4.763139721000
00;3.75000000000000,4.33012701900000;3.25000000000000,4.33012701900000;3,4.76313972
100000;];

xyeq=reshape(xyeq,72,1);
xyeqtemp=[xyeq(2:36); xyeq(38:end)]';


N =36;
adjacency = zeros(N,N);
connections_sparse=sparse([1  1  1  2  2  2  3  3  3  4  4  4  5  5  5  6  6  6  7  7  7  8
8  8  9  9  9  10 10 10 11 11 11 12 12 12 13 13 13 14 14 14 15 15 15 16 16 16 17
17 17 18 18 18 19 19 19 20 20 20 21 21 21 22 22 22 23 23 23 24 24 24 25 25 25
26 26 26 27 27 27 28 28 28 29 29 29 30 30 30 31 31 31 32 32 32 33 33 33 34 34
34 35 35 35 36 36 36],...
                [12 2  14  1  3  16 2  4  17 3  5  19 4  6  20 5  7  22 6  8  23 7  9  25
8  10 26 9  11 28 10 12 29 11 1  13 30 14 12 13 15 1  14 16 32 15 17 2  16 18 3
17 19 33 18 20 4  19 21 5  20 22 34 21 23 6  22 24 7  23 25 35 24 26 8  25 27 9
26 28 36 27 29 10 28 30 11 29 13 31 36 32 30 31 33 15 32 34 18 33 35 21 34 36
24 35 31 27],108);
connections=spones(connections_sparse);
connections=full(connections);
adjacency=connections;
dim=length(adjacency);
onv=[14 16 17 19 20 22 23 25 26 28 29 13];
%
%pleural edge lengths
pleural_edge_length=zeros(length(onv),1);
for n=1:length(onv)-1
    pleural_edge_length(n)=((((xyeq(n+1)-xyeq(n)).^2+(xyeq(n+1+N)- xyeq(n+N)).^2)).^.5);
end
    pleural_edge_length(length(onv))=((((xyeq(1)-xyeq(n+1)).^2+(xyeq(1+N)-
xyeq(n+1+N)).^2)).^.5);


%outer edge lengths
outer_edge_length=zeros(length(onv),1);
for n=1:length(onv)
    outer_edge_length(n)=((((xyeq(onv(n))-xyeq(n)).^2+(xyeq(onv(n)+N)- xyeq(n+N)).^2)).^.5);
```

```matlab
end

%Inner edge lengths
inner_edge_length=((((xyeq(31)-xyeq(30)).^2+(xyeq(31+N)- xyeq(30+N)).^2)).^.5);
l0=zeros(size(adjacency));
%Sections 3+4
for g=length(onv)+1:dim %rows
    for h=1:dim %columns
        if adjacency(g,h)==1
            l0(g,h)=inner_edge_length;
        end
    end
end
%Section 4
for g=onv %rows
    for h=1:length(onv) %columns
        if adjacency(g,h)==1
            l0(g,h)=outer_edge_length(h);
        end
    end
end
%Section 1  all pleural edges
for g=1:length(onv) %rows
    for h=1:length(onv) %columns
        if adjacency(g,h)==1
            l0(h,g)=pleural_edge_length(h);
            l0(g,h)=pleural_edge_length(h);
            l0(length(onv),1)=pleural_edge_length(length(onv));
            l0(1,length(onv))=pleural_edge_length(length(onv));
        end
    end
%Section 2  all outer edges
    for j=length(onv)+1:dim %columns
        if adjacency(g,j)==1
            l0(g,j)=outer_edge_length(g);
        end
    end
end


%%%%%%%K's different L0 the same
% ki=10,
l0=.5.*adjacency;

% ki=10,
kb=(2/7)*(1+sqrt(3))*ki;
ks=(1/6)*(3+2*sqrt(3))*ki;
pleural_edge_k=zeros(length(onv),1);
pleural_edge_k(1:2:end)=kb;
pleural_edge_k(2:2:end)=ks;
%
k=ki*adjacency;

for g=1:length(onv) %rows
    for h=1:length(onv) %columns
```

```
        if k(g,h)==ki;
            k(h,g)=pleural_edge_k(h);
            k(g,h)=pleural_edge_k(h);
        end
    end
end


%%%%%%%Gerneric P
xy(1)=4*anafactor;
xy(N+1)=6.49519052800000*anafactor;


for i=1:N-1
    xy(i+1)=xytemp(i);
    xy(i+N+1)=xytemp(i+N-1);
end

for i =1:N
    for j = 1:N
        if adjacency(i,j)==1
            l(i,j) = sqrt((xy(j)-xy(i))^2+(xy(j+N)-xy(i+N))^2);
            fx(i,j) = k(i,j)*(l(i,j)-l0(i,j))*((xy(j)-xy(i))/l(i,j));
            fy(i,j) = k(i,j)*(l(i,j)-l0(i,j))*((xy(j+N)-xy(i+N))/l(i,j));

        end
    end
end

%%%%%%%Adding puddles to interior nodes via 2*gamma*b
gam=1;
for i =13:N
    for j = 13:N
        if adjacency(i,j)==1
            l(i,j) = sqrt((xy(j)-xy(i))^2+(xy(j+N)-xy(i+N))^2);
            fx(i,j) = fx(i,j)+2*gam*((xy(j)-xy(i))/l(i,j));
            fy(i,j) = fy(i,j)+2*gam*((xy(j+N)-xy(i+N))/l(i,j));

        end
    end
end

%%%%%%%Adding puddles to pleural nodes nodes via gamma*b
for i=1:length(onv)-1
    fx(i+1,i)=fx(i+1,i)+p/2 * (xy(i+N)-xy(i+1+N))+gam*((xy(i)-xy(i+1))/l(i,i+1));
    fx(i,i+1)=fx(i,i+1)+p/2 * (xy(i+N)-xy(i+1+N))+gam*((xy(i+1)-xy(i))/l(i+1,i));
    fy(i+1,i)=fy(i+1,i)+p/2 * (xy(i+1)-xy(i))+gam*((xy(i+N)-xy(i+N+1))/l(i,i+1));
    fy(i,i+1)=fy(i,i+1)+p/2 * (xy(i+1)-xy(i))+gam*((xy(i+N+1)-xy(i+N))/l(i+1,i));

end

lastn=length(onv); %12
fx(1,lastn)=fx(1,lastn) +p/2 * (xy(lastn+N)-xy(N+1))+gam*((xy(lastn)-xy(1))/l(lastn,1));
fx(lastn,1)=fx(lastn,1) +p/2 * (xy(lastn+N)-xy(N+1))+gam*((xy(1)-xy(lastn))/l(1,lastn));
fy(1,lastn)=fy(1,lastn) +p/2 * (xy(1)-xy(lastn))+gam*((xy(N+lastn)-xy(N+1))/l(lastn,1));
fy(lastn,1)=fy(lastn,1) +p/2 * (xy(1)-xy(lastn))+gam*((xy(N+1)-xy(lastn+N))/l(1,lastn));
```

```
for i=1:N

    FX(i)=sum(fx(i,:));
    FY(i)=sum(fy(i,:));
end
FX=FX(2:end)';
FY=FY(2:end)';
FXFYequations=[FX; FY]; %this puts everything in a 70x1vector

end
```

"Jac" calculates the Jacobian.

```
function [J]=wet_SL_jac_seven_hex(p, ki, anafactor,xytemp )
n=length(xytemp);
J=zeros(n,n);
del=.01;
xyperturb=xytemp;
for i=1:n
xyperturb(i)=xyperturb(i)+del;
%Constructs Jacobian by columns (n x n)
J(:,i)=(wet_SL_force_eq_seven_hex(p, ki, anafactor,xyperturb)-wet_SL_force_eq_seven_hex(p,
ki, anafactor,xytemp))/del;
xyperturb(i)=xytemp(i);
end
end
```

"newt_temp" uses a variation on Newton-Raphson method that involves numerical line searching and a numerical solver technique called backtracking to essentially transform NR method into a globally convergent method.

```
function [xynewtemp, new_force]= newt_temp(xynewtemp)

xy=[4,6.49519052800000;4.75000000000000,6.06217782600000;5.25000000000000,5.1961524
2300000;5.25000000000000,4.33012701900000;4.75000000000000,3.46410161500000;4,3.031
08891300000;3,3.03108891300000;2.25000000000000,3.46410161500000;1.75000000000000,
4.33012701900000;1.75000000000000,5.19615242300000;2.25000000000000,6.062177826000
00;3,6.49519052800000;3.25000000000000,6.06217782600000;3.75000000000000,6.06217782
600000;4,5.62916512500000;4.50000000000000,5.62916512500000;4.75000000000000,5.1961
5242300000;4.50000000000000,4.76313972100000;4.75000000000000,4.33012701900000;4.5
0000000000000,3.89711431700000;4,3.89711431700000;3.75000000000000,3.4641016150000
0;3.25000000000000,3.46410161500000;3,3.89711431700000;2.50000000000000,3.897114317
00000;2.25000000000000,4.33012701900000;2.50000000000000,4.76313972100000;2.250000
00000000,5.19615242300000;2.50000000000000,5.62916512500000;3,5.62916512500000;3.25
000000000000,5.19615242300000;3.75000000000000,5.19615242300000;4,4.76313972100000
;3.75000000000000,4.33012701900000;3.25000000000000,4.33012701900000;3,4.7631397210
0000;];
xy=reshape(xy,72,1);
xyini=[xy(2:36); xy(38:end)]';
xynewtemp=xyini;


TOLF=1e-4;
TOLMIN=1e-6;
TOLXY=eps;
STPMX=100;
MAXITS=200;
lam=1;


%%%%Check if initial guess is a root
if max(abs(force_eq_seven_hex( xynewtemp))) < .01*TOLF
    check=0;
    return
end

    NRf=sqrt(sum(force_eq_seven_hex(xynewtemp).^2))/2;

%    stpmax=STPMX*max(abs(xynewtemp),real(size(xynewtemp)));??????

for n=1:MAXITS
    NRg=force_eq_seven_hex(xynewtemp)'*jac_seven_hex(xynewtemp);
    xyoldtemp= xynewtemp;
    NRfold= NRf;
    fvec=(jac_seven_hex(xyoldtemp)\force_eq_seven_hex(xyoldtemp))';
    NRp=-fvec;

    lam=1;
    lam_min=.1;
    alpha=1e-4;
    check=0;
```

```
        slope=dot(NRg,NRp);

        %slope must be negative
        if slope >=0
            warning('Roundoff error in line search')
%            break
        end


while check==0


        xynewtemp= xyoldtemp +lam.*NRp;
        NRf=sqrt(sum(force_eq_seven_hex(xynewtemp).^2))/2;


% if lam<lam_min
%     xynewtemp= xyoldtemp;
%     disp('Break out of line search and let Newt check convergence');
%     check=1;


if NRf < NRfold+(alpha*lam*slope)
    disp('Sufficient function decrease');
    break

else
    if lam==1
        tmplam=-slope/(2*(NRf-NRfold-slope));
    else
        rhs1=NRf-NRfold-lam*slope;
        rhs2=NRf2-NRfold-lam2*slope;
        a=((rhs1/lam^2)-(rhs2/lam2^2))*(1/(lam-lam2));
        b=((-rhs1*lam2/lam^2)+(rhs2*lam/lam2^2))*(1/(lam-lam2));
        if a==0
            tmplam=-slope/(2*b);
        else
            disc=b*b-3*a*slope;
            if disc<0
                tmplam=.5*lam;
            elseif b<=0
                tmplam=(-b+sqrt(disc))/(3*a);
            else
                tmplam=-slope/(-b+sqrt(disc));
            end
        end
        if tmplam>.5*lam
            tmplam=.5*lam;
        end
    end
end
lam2=lam;
NRf2=NRf;
lam=max(tmplam , .1*lam);

end
```

```matlab
    if max(abs(fvec))< TOLF
        check=0;
        break
    end

    if check==1
        check=max(abs(NRg))*max(abs(xynewtemp)) ||  max(f, .5*size(xynewtemp))<TOLMIN;
        break
    end

    if max(abs(xynewtemp-xyoldtemp))/max(abs(xynewtemp))<TOLXY
        break
    end

    new_force(n)=sqrt(sum((force_eq_seven_hex(xynewtemp)).^2));
%       new_force(n)=sum(force_eq_seven_hex(xynewtemp)) ;

end
end
```

APPENDIX C

Plotting larger and more irregular networks can be accomplished by finding the XY points using an image digitizing software. The screenshot below shows the format of a few digitized points of a drawn network. This application is called Plot Digitizer, others include Engague Digitizer, Digitzelt, ORIGIN, and Dagra. Essentially the program will automatically select points from lines and give XY coordinates in exportable format, which can be used in Matlab.
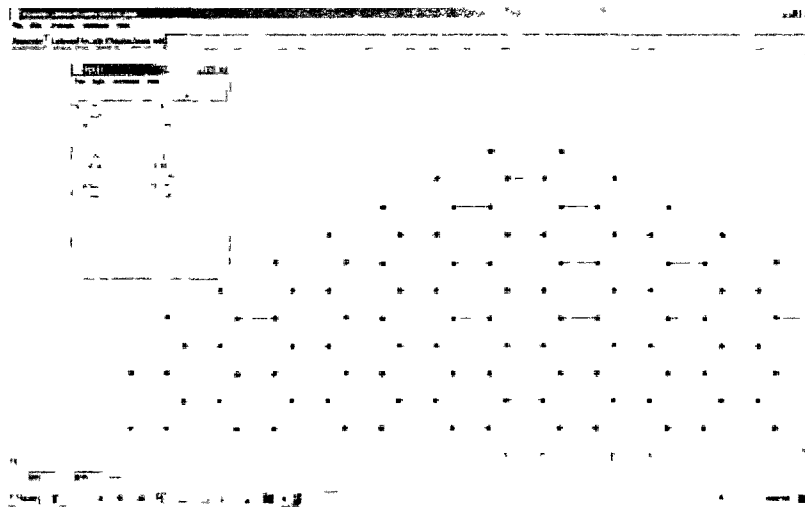

Figure 39: Screenshot of Plot Digitizer

Bibliography

Adler, A. & Bates, J.H., 2000. A micromechanical model of airway-parenchymal interdependence. *Ann Biomed Eng*, 28(3), 309-17.

Ashino, Y. et al., 2000. [Ca(2+)](i) oscillations regulate type II cell exocytosis in the pulmonary alveolus. *Am. J. Physiol. Lung Cell Mol. Physiol*, 279(1), L5-13.

Bachofen, H. et al., 1993. Experimental hydrostatic pulmonary edema in rabbit lungs. Morphology. *Am. Rev. Respir. Dis*, 147(4), 989-96.

Bates, J.H., 2007. A recruitment model of quasi-linear power-law stress adaptation in lung tissue. *Ann Biomed Eng*, 35(7), 1165-74.

Bautista, D., Machen, T. & Hariharan, I., 2011. Advanced Physiology: Physiology of Respiration.

Brewer, K.K. et al., 2003. Lung and alveolar wall elastic and hysteretic behavior in rats: effects of in vivo elastase treatment. *J. Appl. Physiol*, 95(5), 1926-36.

Brown, A., 2010. Respiratory Physiology Problems Respiratory Ventilation.

Cavalcante, F.S. et al., 2005. Mechanical interactions between collagen and proteoglycans: implications for the stability of lung tissue. *J. Appl. Physiol*, 98(2), 672-9.

Centers for Disease Control and Prevention, 2010. Fast Stats: Asthma.

Centers for Disease Control and Prevention, 2011. Fast Stats: Chronic Obstructive Pulmonary Disease.

DiRocco, J.D. et al., 2006. Dynamic alveolar mechanics in four models of lung injury. *Intensive Care Med*, 32(1), 140-8.

European Lung Foundation, 2011. The Lung: Images.

Faffe, D.S. & Zin, W.A., 2009. Lung parenchymal mechanics in health and disease. *Physiol. Rev*, 89(3), 759-75.

Flicker, E. & Lee, J.S., 1974. Equilibrium of force of subpleural alveoli: implications to lung mechanics. *J Appl Physiol*, 36(3), 366-74.

Fredberg, J. & Kamm, R., 2006. Stress transmission in the lung: pathways from organ to molecule. *Annu. Rev. Physiol*, 68, 507-41.

Fung, Y.C., 1975a. Does the surface tension make the lung inherently unstable?. *Circ. Res*, 37(4), 497-502.

Fung, Y.C., 1975b. Stress, deformation, and atelectasis of the lung. *Circ. Res*, 37(4), 481-96.

Fung, Y.C. & Sobin, S.S., 1972. Elasticity of the pulmonary alveolar sheet. *Circ. Res*, 30(4), 451-69.

Gardel, M.L. et al., 2004. Elastic behavior of cross-linked and bundled actin networks. *Science*, 304(5675), 1301-5.

Gatto, L.A. & Fluck, R.R., 2004. Alveolar mechanics in the acutely injured lung: role of alveolar instability in the pathogenesis of ventilator-induced lung injury. *Respir Care*, 49(9), 1045-55.

Gibson, L. & Ashby, M., 1997. Cellular solids: structure and properties, Cambridge, UK: Cambridge University Press.

Gil, J., 1983. Alveolar surface, intra-alveolar fluid pools, and respiratory volume changes. *Journal of Applied Physiology*, (Letters to the Editor).

Guyton, C... & Hall, E., 1996. Textbook of Medical Physiology Nineth., Philadelphia, PA: W.B. Saunders Company.

Hamm, H., Kroegel, C. & Hohlfeld, J., 1996. Surfactant: a review of its functions and relevance in adult respiratory disorders. *Respir Med*, 90(5), 251-70.

Hills, B.A., 1999. An alternative view of the role(s) of surfactant and the alveolar model. *J. Appl. Physiol*, 87(5), 1567-83.

Hoppin, F. et al., 1998. Lung recoil: elastic and rheological properties. In P. Macklem & J. Mead *Handbook of Physiology: Section 3 The Respiratory System, Part 1 Mechanics of Breathing*. An American Physiological Society Book, p 195.

Hubmayr, R.D., 2002. Perspective on lung injury and recruitment: a skeptical look at the opening and collapse story. *Am. J. Respir. Crit. Care Med*, 165(12), 1647-53.

Hung, G., Fiedler, A. & Ciuffreda, K., 2010. Homeomorphic Matlab Model of Myopia Development. *Journal of Computer Science and Systems Biology*, 3, 030-039.

Ingenito, E.P. et al., 2005. On the role of surface tension in the pathophysiology of emphysema. *Am. J. Respir. Crit. Care Med*, 171(4), 300-4.

Johns Hopkin's School of Medicine, 1995. Interactive Respiratory Physiology: Alveolar Pressure.

Karakaplan, A.D., Bieniek, M.P. & Skalak, R., 1980. A mathematical model of lung parenchyma. *J Biomech Eng*, 102(2), 124-36.

Kitaoka, H., Takaki, R. & Suki, B., 1999. A three-dimensional model of the human airway tree. *J. Appl. Physiol*, 87(6), 2207-17.

Lai-Fook, S.J. & Hyatt, R.E., 2000. Effects of age on elastic moduli of human lungs. *J. Appl. Physiol*, 89(1), 163-8.

MD Guidelines, 2000. Pulmonary Edema.

Mead, J., 1973. Respiration: pulmonary mechanics. *Annu. Rev. Physiol*, 35, 169-92.

Mead, J., Takishima, T. & Leith, D., 1970. Stress distribution in lungs: a model of pulmonary elasticity. *J Appl Physiol*, 28(5), 596-608.

Pelosi, P. & Rocco, P.R., 2008. Effects of mechanical ventilation on the extracellular matrix. *Intensive Care Med*, 34(4), 631-9.

Perlman, C.E. & Bhattacharya, J., 2007. Alveolar expansion imaged by optical sectioning microscopy. *J. Appl. Physiol*, 103(3), 1037-44.

Prange, H.D., 2003. Laplace's Law and the alveolus: a misconception of anatomy and a misapplication of physics. *Adv Physiol Educ*, 27(1-4), 34-40.

Press, W. et al., 2007. Numerical Recipes: The Art of Scientific Computing Third., Cambridge: Cambridge University Press.

Pulmonary Fibrosis Foundation, 2011. Prevalence of Pulmonary Fibrosis.

Raghavan, V., 2004. Materials Science and Engineering: A First Course 5th., New Delhi: Prentice Hall.

Ricci, S.B. et al., 2002. Mechanical model of the inspiratory pump. *J Biomech*, 35(1), 139-45.

Rice, W.R., 2000. Life in the alveolus: who's in charge?. *Am. J. Physiol. Lung Cell Mol. Physiol*, 279(1), L3.

Sakai, H. et al., 1999. Acute response of the lung mechanics of the rabbit to hypoxia. *J. Appl. Physiol*, 86(1), 306-12.

Salerno, F.G. & Ludwig, M.S., 1999. Elastic Moduli of excised constricted rat lungs. *Journal of Applied physiology*, 86(1), 66-70.

Scarpelli, E.M. & Hills, B.A., 2000. Opposing views on the alveolar surface, alveolar models, and the role of surfactant. *J. Appl. Physiol*, 89(2), 408-12.

SpirXpert: Philip H. Quanjer,1999. Airway structure and function.

Suki, B. et al., 2005. Biomechanics of the lung parenchyma: critical roles of collagen and mechanical forces. *J. Appl. Physiol*, 98(5), 1892-9.

Suki, B. & Bates, J.H., 2008. Extracellular matrix mechanics in lung parenchymal diseases. *Respir Physiol Neurobiol*, 163(1-3), 33-43.

Tanaka, R. & Ludwig, M.S., 1999. Changes in viscoelastic properties of rat lung parenchymal strips with maturation. *J. Appl. Physiol*, 87(6), 2081-9.

The ARDS Foundation, 2011. Acute Respiratory Distress Syndrome.

Tschumperlin, D.J., Boudreault, F. & Liu, F., 2010. Recent advances and new opportunities in lung mechanobiology. *J Biomech*, 43(1), 99-107.

Vawter, D.L., Matthews, F.L. & West, J.B., 1975. Effect of shape and size of lung and chest wall on stresses in the lung. *J Appl Physiol*, 39(1), 9-17.

Weibel, E.R., 2008. How to make an alveolus. *Eur. Respir. J*, 31(3), 483-5.

West, B., 2005. Respiratory Physiology: The essentials Seventh., Baltimore, Maryland: Lippincott Williams & Wilkins.

Wilson, T.A., Anafi, R.C. & Hubmayr, R.D., 2001. Mechanics of edematous lungs. *J. Appl. Physiol*, 90(6), 2088-93.

Yuan, H. et al., 2000. Effects of collegenase and elastase on the mechanical properties of lung tissue strips. *Journal of Applied Physiology*, 89(1), 3-14.